Role of redox conditions and thermal metamorphism in the preservation of Cr isotopic anomalies in components of non-carbonaceous chondrites

Paul Frossard, Pierre Bonnand, Maud Boyet, Audrey Bouvier

Role of redox conditions and thermal metamorphism in the preservation of Cr isotopic anomalies in components of non-carbonaceous chondrites

Paul Frossard[1,2], Pierre Bonnand[1,3], Maud Boyet[1], Audrey Bouvier[4]
1 Université Clermont Auvergne, CNRS, IRD, OPGC, Laboratoire Magmas et Volcans, F-63000 Clermont-Ferrand, France
2 Institute of Geochemistry and Petrology, ETH Zürich, Zürich, Switzerland
3 Université de Bretagne Occidentale, CNRS, IFREMER, Laboratoire Géo-Océan, Plouzané, France
4 Bayerisches Geoinstitut, Universität Bayreuth, 95447 Bayreuth, Germany

Abstract

Mass-independent isotopic anomalies in meteorites are probes to the dynamics and evolution of the protoplanetary disc and the reservoirs from which planetary bodies accreted. Variable Cr nucleosynthetic compositions between meteorite groups are observed but the cause is not well understood. Investigations on presolar carriers in unequilibrated chondrites are thus required to establish these relationships. For that purpose, we analysed the Cr isotope compositions of leachates (stepwise dissolution solutions) of one ordinary chondrite and two enstatite chondrites of EL and EH subgroups previously measured for Nd and Sm isotopes. The leachates of the ordinary chondrite display large variations of their Cr isotope compositions, whereas the leachates of the enstatite chondrites show very limited variations of their nucleosynthetic compositions, confirming other studies. The Cr isotope compositions of leachates of unequilibrated chondrites are significantly modified by thermal processing and aqueous alteration under various conditions. The leachates of the enstatite chondrites are relatively homogeneous for Cr isotope composition, suggesting that presolar carriers of Cr are not stable under very reduced conditions and are likely oxidised phases. After careful examination of the role of parent body processing, we conclude that there is one predominant presolar carrier enriched in ^{54}Cr that produced most of the nucleosynthetic variations observed in leachates. This carrier is likely depleted in the carbonaceous reservoir relative to the non-carbonaceous reservoir. The drastically different isotope compositions of Cr and heavy refractory lithophile elements such as Nd of leachates of chondrites reflect relative preservation biases of their respective presolar carriers, namely a still poorly characterised presolar oxide and silicon carbide (SiC), respectively.

Keywords: Cr isotope composition, nucleosynthetic anomalies, ^{54}Cr, redox, thermal metamorphism, enstatite chondrites, ordinary chondrites.

1. Introduction

The mass-independent isotopic compositions of many elements in meteorites provide clues on the dynamics in the early solar system and the formation of planets. Chromium is particularly well-suited for this purpose because different nucleosynthetic sources have been proposed for its four isotopes (e.g. Clayton, 2003). The ^{53}Mn-^{53}Cr short-lived radionuclide system (half-life of 3.7 Ma) provides a useful chronometer of early cosmochemical events (e.g. Birck and Allègre, 1985; Glavin et al., 2004). The Mn-Cr chronometry is particularly advantageous in meteorites such as enstatite chondrites (e.g., Wadhwa et al., 1997; Shukolyukov and Lugmair, 2004), when the more traditional Al-Mg and U-Pb systematics are not so suitable owing to the lack of Al- or U-rich accessory minerals. The ^{53}Mn-^{53}Cr chronometer is also useful for determining the age of carbonates providing constraints on the timing of aqueous alteration in carbonaceous chondrites (e.g., de Leuw et al., 2009; Fujiya et al., 2012). The precise dating of chondrules and chondrite accretion is however prone to disturbance due to thermal metamorphism, nucleosynthetic anomalies and exposure to galactic cosmic rays (e.g. Posner et al., 2016; Dauphas et al., 2010; Kadlag et al., 2021). Igneous crystallisation, magma ocean crystallisation and volatile element loss on planetesimals can be dated due to the different geochemical behaviours and volatilities of Mn and Cr, with 50% condensation temperature for Mn (1123 K) compared to Cr (1291 K) (Wood et al., 2019). Whether there was a homogeneous distribution of ^{53}Mn in the solar system is still debated and relies upon a good understanding of the non-radiogenic ^{53}Cr abundance (e.g. Birck et al., 1999; Lugmair and Shukolyukov, 1998; Shukolyukov and Lugmair, 2000, 2004, 2006; Trinquier et al., 2008; Yamashita et al., 2010).

Chromium nucleosynthetic anomalies carry information on the origin and evolution of material in the protoplanetary disc. Meteorites from various groups display different isotope compositions for many elements including Cr (e.g. Trinquier et al., 2007; Bermingham et al., 2020). The comparison of Cr, Ti and O isotope compositions of meteorites has been a cornerstone of the discovery of a compositional dichotomy between non-carbonaceous meteorites (NC), comprising enstatite, ordinary, Rumuruti and Kakangari chondrites as well as most achondrites (including iron meteorites), and carbonaceous meteorites (CC), comprising all carbonaceous chondrites as well as a few ungrouped achondrites and primitive achondrites (Trinquier et al., 2007; Leya et al., 2008; Warren, 2011; Bermingham et al., 2020; Ma et al., 2022). This dichotomy putatively corresponds to inner and outer solar system materials. Some studies propose that these reservoirs remained separated by Jupiter or pressure gaps (Kruijer et al., 2017; Alibert et al., 2018; Brasser and Mojzsis, 2020), whereas others, for instance, highlight that these reservoirs may have formed at different times and may not have been isolated from each other (Williams et al, 2020; Lichtenberg et al., 2021). Nucleosynthetic anomalies for Cr are determined using the ^{54}Cr/^{52}Cr, expressed as ε units as the deviation from the terrestrial standard (NIST SRM 979) in parts per 10 000. On one hand, NC meteorites are characterised by negative anomalies in ε^{54}Cr, ranging from - 0.8 in ureilites to 0 in enstatite chondrites, which ε^{54}Cr are similar to that of the Earth (Trinquier et al., 2007). On the other hand, CC meteorites contain excesses of ^{54}Cr compared to NC meteorites and range from 0.4 to 1.6 ε^{54}Cr (Zhu et al., 2021).

The origin of the different compositions and end-members in meteorite groups is however little understood. Chromium nucleosynthetic anomalies in bulk meteorites require anomalous components that are heterogeneously distributed. The processes that have been invoked to produce this heterogeneity include physical sorting of grains (e.g. Dauphas et al., 2014), thermal processing (e.g. Trinquier et al., 2009) and injection of supernova material to the protoplanetary disc (e.g. Qin et al., 2011b). In terms of stellar origin, ^{50}Cr, ^{52}Cr and ^{53}Cr are produced by quasi-equilibrium explosive burning of oxygen and silicon in supernovæ (SN) of type I and II. A different setting is thought to produce ^{54}Cr, namely by quasi-equilibrium in neutron-rich regions of type Ia supernovæ (SNIa), similarly to other neutron-rich isotopes such as ^{50}Ti and ^{48}Ca (Clayton, 2003). Measurements of ^{54}Cr-rich presolar oxides from chondrites have highlighted that SNII were a likely source for these grains (Dauphas et al., 2010; Qin et al., 2011b) but some SNIa or electron-capture SN (ECSN) are favoured by coupled Cr and Ti isotope measurements of these grains (Nittler et al., 2018).

The sequential dissolution (or leaching experiment) method makes it possible to isolate chemical components of chondrites, thereby increasing the possibility of identifying components with anomalous compositions, e.g. nucleosynthetic carriers. The pioneering work of Rotaru et al. (1992) showed large ^{54}Cr anomalies up to 100 ε units in leachates of carbonaceous chondrites. Several studies confirmed the presence of highly anomalous ^{54}Cr-rich components (Podosek et al., 1997; Trinquier et al., 2007, 2008; Dauphas et al., 2010; Qin et al., 2011a; Wang et al., 2011; Petitat et al., 2011; Schiller et al., 2014; Yamakawa and Yin, 2014; Göpel et al., 2015). The largest anomalies were identified in CI chondrites. It also appeared that anomalies were not distributed in the same manner between different CC chondrite sub-groups (Rotaru et al., 1992; Trinquier et al., 2007). A few leaching studies have investigated NC chondrites, comprising two studies of ordinary chondrites (Qin et al., 2011a; Wang et al., 2011) and two studies of enstatite chondrites (Qin et al., 2010; Kadlag et al., 2021). Qin et al. (2010) performed a partial leaching procedure and Kadlag et al. (2021) performed a full leaching procedure. Leachates from ordinary chondrites displayed anomalies in the order of a few ε units, whereas very little variation was observed in enstatite chondrites (< 1ε).

The present study expands the Cr isotope composition dataset of leaching experiments of NC chondrites with samples for which Nd and Sm isotope compositions have already been reported (Frossard et al., 2022). The aim is to understand the origin of heterogeneous nucleosynthetic Cr isotopic compositions in bulk meteorites and understand the effects of high-temperature processing in different redox conditions for Cr and compare with other elements. To this end, we analysed the Cr isotope composition of leachates of a L3.2 ordinary chondrite and two type 3 EH and EL enstatite chondrites. Processes that produced the Cr isotope composition of these leachates are discussed and we assess whether chronological and nucleosynthetic information can be derived from them. Finally, we review the literature data on leachates of chondrites that formed in different environments and identify how physico-chemical conditions may affect their Cr isotope compositions.

2. Methods

Three unequilibrated chondrite samples of the NC reservoir were sequentially leached in this study. The enstatite chondrites Sahara 97158 (EH3), Pecora Escarpment (PCA) 91020 (EL3) and the ordinary chondrite Northwest Africa (NWA) 8007 (L3.2) were chosen based on their low metamorphic and low weathering grades. The fragment PCA 91020,88 was provided by the Antarctic Meteorite Collection whereas NWA 8007 and Sahara 97158 were purchased from private meteorite dealers. The detailed procedure of the leaching and dissolution steps is described in Frossard et al. (2022). A summary is presented in this section.

Interior parts of the chips without fusion crust were selected and cleaned in ethanol. The samples were then powdered in an agate mortar. The leaching procedure was applied on 1.2 to 1.5 g of sample powder. Acids of increasing strength were poured onto powders, then pipetted out and centrifuged after reaction for a given duration and at a given temperature. The leaching procedure is detailed in Table 1. Leachates were then dried down and dissolved in 7 M HNO_3, dried down once again and finally dissolved in 6 M HCl and evaporated to dryness. In addition to leachates, separates from the EH3 Sahara 97158 were also prepared. The sample was gently crushed, and two fractions were separated using a hand magnet. The magnetic separate (Mag) consists of metal as well as metal-sulphide nodules, whereas the non-magnetic separate (NM) consists of silicates and chondrules. An aliquot of 1 % was saved from the total solutions for Cr isotope analysis.

The Cr separation procedure is adapted from that of Trinquier et al. (2008) and Bonnand et al. (2011, 2016) and is performed in two steps. The first step consists of removing major elements using 2 mL of AG50W-X8 resin (200-400 mesh) in Polyprep Biorad columns. Before use, the resin is cleaned with 30 mL of 6 M HCl and conditioned in 10 mL of 1 M HCl. Samples are dissolved in 6 M HCl and heated for 12 hours on a hotplate at 145 °C and diluted to 1 M HCl just before loading in a 4 mL volume of solution. Six mL of 1 M HCl are then added. The Cr cut (85-90 % of total Cr) corresponds to the 10 mL eluted in 1 M HCl including loading. Matrix elements are then eluted in 18 mL 6 M HCl, in which 10-15 % of Cr is also eluted (Trinquier et al., 2008; Bonnand et al., 2011). This second Cr peak is related to different Cr chloride species that form during this procedure (Trinquier et al., 2008; Larsen et al., 2016). The pre-treatment with 6 M HCl at 145°C should alleviate this issue by ensuring that Cr is present in the solution only as $CrCl_2^+$ in Cr(III) oxidation state (Larsen et al., 2016). The effect of this incomplete separation on the Cr isotope compositions is detailed below. The second column isolates Cr from minor elements, in particular from isobaric elements Ti and V, using 1 mL of the AG-50W-X8 resin in Polyprep Biorad columns. The resin is cleaned with 10 mL of 3 M HNO_3, followed by 30 mL of 6 M HCl, and finally conditioned with 10 mL of 0.5 M HNO_3. The sample is dissolved in 14 M HNO_3 and diluted to 4 mL of 0.5 M HNO_3 and heated for 2 hours at 110 °C prior to loading. The resin is then rinsed with 4 mL of 0.5 M HNO_3, 6 mL of 1 M HF to remove Ti, and 7 mL of 1 M HCl to remove minor matrix elements. Chromium is eluted in 6 mL of 6 M HCl. Due to the imperfect separation of major elements, some leachates were further purified using the same procedure one more time. In order to keep similar conditions for all samples, amounts of sample

corresponding to 1.5 μg of Cr were loaded on the columns with the exception of Cr-depleted leachates containing between 0.3 and 1.2 μg of Cr for which the complete samples were used. Total yields of the procedure are around 85 % and blank contributions are between 0.1 to 0.6 ng, therefore negligible compared to the Cr amounts processed for all samples.

The concentrations of Mn, Cr and Fe in the samples were measured with a Q-ICP-MS Agilent 7500 at Laboratoire Magmas et Volcans (LMV). The Fe contents were only measured for leachates of Sahara 97158. The concentrations were obtained with external calibration using multi-element synthetic standard solutions of different concentrations ranging from 1 to 25 ppb. The trace element composition of leachates are reported in Frossard et al. (2022).

Following purification, the sample is dissolved in 14 M HNO_3 and 30 % H_2O_2 and dried twice to remove organics from the resin. The loading procedure is described in Bonnand et al. (2016) and adapted from Trinquier et al. (2008). One microgram of Cr, or less for samples with lower contents, was loaded in 6 M HCl onto Re single filaments at 0.7 A and evaporated before adding a silica gel solution saturated in boric acid and "flashed" to form a glass. Measurements of the Cr isotope compositions of samples were performed on a ThermoScientific Triton TIMS at LMV using a multi-static method. The latter consists of three lines of measurements centred successively on ^{52}Cr, ^{53}Cr and ^{51}V. The whole analysis is generally composed of 27 blocks of 20 cycles of 8 s of integration time. Samples and standards were run in similar conditions with intensities of about 1×10^{-10} A of ^{52}Cr. Isotope ratios are corrected for mass fractionation using a $^{50}Cr/^{52}Cr$ ratio of 0.051859 (Shields et al., 1966) and an exponential law. Mass-independent ratios are calculated for each line and the mean of the three ratios obtained for each cycle calculated. The sample isotope composition reported is the mean of all cycles. Interference contributions are corrected for Fe and are negligible for Ti and V. The contribution of Fe is monitored on line 2 with ^{56}Fe and extrapolated for lines 1 and 3, similarly to the method of Trinquier et al. (2008). Corrections for $^{54}Cr/^{52}Cr$ from ^{54}Fe are generally at the ppm level with $^{56}Fe/^{52}Cr$ around 10^{-6}.

Isotope ratios are reported as a deviation relative to the mean composition of the NIST SRM 979 standards processed through chemistry (NIST SRM 979*) in parts per 10 000, or ε, following this equation:

$$\varepsilon\ ^{i}Cr = \left(\frac{^{i}Cr}{^{52}Cr}_{measured} \Big/ \frac{^{i}Cr}{^{52}Cr}_{NIST\ SRM\ 979^{*}} - 1 \right) \times 10\,000$$

Mass-independent fractionation that remains after correction by exponential law complicates Cr isotope analyses. This results in a correlation of $^{53}Cr/^{52}Cr$ and $^{54}Cr/^{52}Cr$. Several authors identified the issue and interpreted it as a fractionation due to the two Cr chloride species in the first chemical separation on AG50W-X8 resin (Trinquier et al., 2008, Van Kooten et al., 2016) and due to evaporation of Cr^+ and CrO^+ ionic species on the filament during analysis (Bourdon and Fitoussi, 2020; Cornet et al., 2022; Yokoyama et al., 2023). We measured the isotope composition of 16 NIST SRM 979 standards without chemical separation and 12 NIST SRM 979 standards that underwent the same chemical procedure as the samples (Table 2).

A correlation is observed among NIST SRM 979 runs, similarly to other studies (e.g. Trinquier et al., 2008) (Figure 1). The Cr isotope compositions of processed and unprocessed NIST SRM 979 standards display the same trend, with a slope of 2.6 ± 0.4 in $\varepsilon^{54}Cr$-$\varepsilon^{53}Cr$ space (95 % confidence interval, model 3 IsoplotR, Vermeesch, 2018). Mass-independent fractionations during chemical separation and TIMS analyses are produced by the nuclear field shift effect and incompletely corrected mass-dependent equilibrium or kinetic fractionations. The mass-independent fractionation induced by the nuclear field shift effect is characterised by a $\varepsilon^{54}Cr/\varepsilon^{53}Cr$ ratio of 2.53 calculated using the equations of Fujii et al. (2006), nuclei masses from Wang et al. (2012) and mean-squared nuclear charge radii of Fricke and Heilig (2004). Larsen et al. (2016) reported that the Cr isotope composition of samples with incomplete recovery of chloride species $CrCl^{2+}$, $CrCl_2^+$ and $CrCl_3^0$ is prone to equilibrium isotope fractionation that is incorrectly corrected by the exponential mass fractionation law. The fractionation of NIST SRM 979 reported in this study is also in part induced during analysis, as exemplified by the trend observed in the unprocessed standards. This effect was also highlighted in previous studies (e.g. Trinquier et al., 2008; Qin et al., 2010; Bourdon and Fitoussi, 2020; Cornet et al., 2022). Depending on the conditions of evaporation on the filament, oxides are formed in different amounts. The different CrO^+/Cr^+ ratios induce mass-independent fractionations consistent with the nuclear field shift effect as shown by the slope described in our data (Yokoyama et al., 2023). The temperature of the filament is a primordial parameter in that regard (Yokoyama et al., 2023). Processed standards were generally analysed at higher temperatures (1256-1310 °C) than the unprocessed standards (1243-1281 °C). The difference between the Cr isotope composition of processed and unprocessed sets of standards is 5.3 ppm for $^{53}Cr/^{52}Cr$ and 12.8 ppm for $^{54}Cr/^{52}Cr$ ratios. The offsets are attributed to fractionation during the chemical procedure and the analysis on the TIMS.

Consequently, as in Bonnand et al. (2016) the samples' Cr isotope compositions were normalised to standards that underwent chemical separation to correct for the fractionation related to the chemical procedure. However, this does not include the mass-independent fractionation that occurs during evaporation on the filament. This variation is nevertheless included in the error with repeated measurements of processed standards. The uncertainties reported for the samples correspond to twice the standard deviation on 12 processed NIST SRM 979 standards, or twice the standard error on one run if it is larger than the reproducibility. The reproducibility on the NIST SRM 979 is 6.1 ppm for $\varepsilon^{53}Cr$ and 17.6 ppm for $\varepsilon^{54}Cr$.

The reproducibility and accuracy of the chemical procedure and the measurements are assessed using the terrestrial peridotite rock standard JP-1 and chondrites Indarch (EH4) and Barratta (L5) from the same powder aliquot reported by Bonnand et al. (2016). They yield similar results to the literature reporting the Cr isotope composition of these samples and other enstatite and ordinary chondrites using different methods (e.g. Qin et al., 2010; Yamakawa and Yin, 2014; Bonnand et al., 2016; Hibiya et al., 2019). Indeed, Indarch displays $\varepsilon^{53}Cr$ of 0.19 ± 0.06 and 0.23 ± 0.06 and $\varepsilon^{54}Cr$ of -0.01 ± 0.18 and 0 ± 0.18, whereas Barratta displays $\varepsilon^{53}Cr$ of 0.22 ± 0.06 and 0.20 ± 0.06 and $\varepsilon^{54}Cr$ of -0.34 ± 0.18 and -0.41 ± 0.18.

3. Results

The Cr isotope compositions of the samples are reported in Table 2 and are presented in Figures 2-4. The enstatite chondrite leachates are characterised by a large range of $\varepsilon^{53}Cr$, from 0.11 ± 0.06 (Sahara 97158 L5) to 1.66 ± 0.06 (Sahara 97158 L1) that are loosely correlated with their corresponding $^{55}Mn/^{52}Cr$ ratios (Figure 3). The variations in $\varepsilon^{53}Cr$ are larger in the leachates of the EH3 Sahara 97158 than those of the EL3 PCA 91020. However, there is less variation in the $\varepsilon^{54}Cr$ composition of the leachates of the enstatite chondrites, ranging from -0.20 ± 0.18 (PCA 91020 L3) to 0.52 ± 0.18 (PCA 91020 L1) (Figure 4). The leaching steps of EL3 and EH3 chondrites are close in $\varepsilon^{54}Cr$ compositions, but present resolved variations. The first leachates (L1) obtained with 0.5 M acetic acid display the same $\varepsilon^{54}Cr$ composition for EH3 and EL3, but $\varepsilon^{54}Cr$ anomalies in leachates L2 and L3 are systematically lower for the EL3. Similarly, the last leachate (L6) of the EL3 displays a $\varepsilon^{54}Cr$ composition of 0.48 ± 0.18, whereas the last leachate of the EH3 has a composition that is terrestrial within error (0.19 ± 0.18). The separates from the EH3 chondrite Sahara 97158 have Cr isotope compositions that are very similar to the bulk enstatite chondrite composition from the literature. The non-magnetic fraction displays a $\varepsilon^{53}Cr$ of 0.12 ± 0.06, lower than the bulk EC and the magnetic fraction, which is probably related to its low $^{55}Mn/^{52}Cr$ ratio of 0.65.

The Cr isotope composition of the leachates of the ordinary chondrite NWA 8007 contrasts with that of enstatite chondrite leachates. The $\varepsilon^{53}Cr$ composition of leachates also loosely correlates with $^{55}Mn/^{52}Cr$. The $\varepsilon^{54}Cr$ composition of OC leachates displays very large deficits up to -6.68 ±0.18 with excesses that are well resolved for L5 and L6 of 0.84 ± 0.18 and 0.56 ± 0.18, respectively (Figure 5). L1 and L2 leachates display $\varepsilon^{54}Cr$ compositions around -1.5, whereas deficits are larger for L3 and L4.

4. Discussion

4.1 Galactic cosmic ray effects

Meteorite samples exposed to galactic cosmic rays (GCR) display altered Cr isotope compositions. GCR exposure produces excesses in both $\varepsilon^{53}Cr$ and $\varepsilon^{54}Cr$ as exemplified by the Cr isotope composition of iron meteorites (e.g. Leya et al., 2003; Qin et al., 2010; Bonnand and Halliday, 2018; Liu et al., 2019). The cosmogenic production of Cr isotopes varies with several parameters such as the Cr, Ni, and Fe concentrations in the sample, the particle flux, the duration of exposure, and the shielding depth. It consists primarily of spallation reactions on Fe, Ni and Cr and neutron capture on Cr isotopes (Leya et al., 2003; Liu et al., 2019). The bulk Cr isotope compositions of chondrites are relatively little affected by cosmic rays (e.g. Qin et al., 2010). The modelled effects of the GCR on Cr isotope compositions from Leya et al. (2003) with different Fe/Cr ratios and from Liu et al. (2019) in iron meteorites do not correspond to the range of compositions of leachates of chondrites. GCR effects on $\varepsilon^{53}Cr$ and $\varepsilon^{54}Cr$ may vary depending on the nature of the reactions, i.e. spallation reaction or neutron capture. Samarium isotope compositions indicate the degree of epithermal neutron capture because of the large cross-section of ^{149}Sm. Neutron capture effects are relatively mild in the meteorites investigated according to their small deficits of ^{149}Sm and excesses of ^{150}Sm (Frossard et al., 2022). Variations in the Cr isotope compositions of the ordinary chondrite leachates

are relatively large and a GCR contribution can be ruled out to explain deviations up to 6.68 ε units from the terrestrial reference.

In contrast, small variations can be attributed to GCR in enstatite chondrite leachates (Kadlag et al., 2021). This interpretation stems from the well-defined correlation between $\varepsilon^{54}Cr$ and Fe/Cr in separates and leachates. Some isotopes of Fe and Ni produce Cr isotopes due to spallation reactions and Fe/Cr ratios are often used as indicators of irradiation effects when compared with Cr isotope compositions. In our study, the magnetic separate (Mag) that includes metal-sulphide nodules of the EH3 Sahara 97158 chondrite displays small excesses in $\varepsilon^{53}Cr$ and $\varepsilon^{54}Cr$ compared to the non-magnetic fraction (NM) (Figure 2). Iron contents were measured only in the leachates and separates of Sahara 97158 (EH3) and the leachates of the ordinary chondrite NWA 8007 (L3.2). The leachates and separates of Sahara 97158 generally follow the same trend as the data from Kadlag et al. (2021) (Figure 6). The information from the Fe/Cr of leachates of Sahara 97158 may not be reliable as Fe and Cr in leachates are likely decoupled from measured Cr isotope compositions based on the different solubilities of Fe and Cr. Nevertheless, excesses of ^{54}Cr correlate with Fe/Cr in sorted fractions (that did not experience leaching) of the EH3 chondrites Kota-Kota and Sahara 97072 (Kadlag et al., 2021) with a similar slope. This is evidence for a GCR origin of the $\varepsilon^{54}Cr$ deviations in enstatite chondrites. The relationship between Fe/Cr and $\varepsilon^{53}Cr$ is not as clear because leachates or separates with high Mn/Cr ratios also display high $\varepsilon^{53}Cr$, which are larger than the anticipated GCR effects.

Spallation appears to be the main cause of the $\varepsilon^{54}Cr$ variability of leachates in enstatite chondrites and to some extent $\varepsilon^{53}Cr$. Despite undoubtably holding a main role in explaining the Cr isotope compositions of components of enstatite chondrites, irradiation may not explain the differences in bulk meteorites or planetary bodies as hypothesised by Kadlag et al. (2021). The main reason is that $\varepsilon^{54}Cr$ and $\varepsilon^{50}Ti$ are correlated in NC materials and that irradiation has little effects on Ti isotopes (Leya et al., 2008). The origin of this relationship is most likely related to heterogeneous distribution of nucleosynthetic anomalies in the protoplanetary disc (Leya et al., 2008; Trinquier et al., 2009).

4.2 $\varepsilon^{53}Cr$ variations in leachates of unequilibrated ordinary and enstatite chondrites

Variations in the $\varepsilon^{53}Cr$ composition of leachates of ordinary and enstatite chondrites from this study show that they formed during the lifetime of ^{53}Mn, i.e. in the first 20 million years after the crystallization of Ca, Al-rich inclusions (CAI). Nevertheless, relationships between $\varepsilon^{53}Cr$ and $^{55}Mn/^{52}Cr$ ratios are not well defined and display significant scatter along regression lines (Figure 3). Dating unequilibrated chondrites with leachates is complicated by several issues: Mn and Cr may be leached differently at each step of the leaching procedure and Mn/Cr ratios may not be in equilibrium with the measured Cr isotopic compositions. Nucleosynthetic anomalies hosted in components of chondrites may also affect the $\varepsilon^{53}Cr$ compositions of leachates. Finally, mixing between different components may blur the potential relationships between $\varepsilon^{53}Cr$ and $^{55}Mn/^{52}Cr$ (Göpel et al., 2015).

The regression line obtained with leachates of the ordinary chondrite NWA 8007 yields an initial $^{53}Mn/^{55}Mn$ ratio of 2.3×10^{-6} that is less than half of the $^{53}Mn/^{55}Mn$ ratio of $5.1 \pm 1.6 \times 10^{-6}$ inferred form

chondrules from the primitive ordinary chondrite LL3.4 Chainpur (Yin et al., 2007). However, this slope cannot be used to define an initial $^{53}Mn/^{55}Mn$ ratio due to the scatter that indicates that $\varepsilon^{53}Cr$ variations are not solely related to the decay of ^{53}Mn. The large variations in $\varepsilon^{54}Cr$ in this meteorite suggest that nucleosynthetic anomalies may impede the correct quantification of radiogenic ^{53}Cr. In the absence of precise constraints on the $\varepsilon^{53}Cr$ composition of presolar carriers, an evaluation of this contribution is not possible. Note that small nucleosynthetic anomalies have been reported in $\varepsilon^{53}Cr$ in previous studies on leachates of carbonaceous chondrites (e.g. Trinquier et al., 2008; Yamakawa and Yin, 2014; Göpel et al., 2015).

Concerning enstatite chondrites, the dispersion of isochron diagrams is significant. The slope of the regression line is principally controlled by the composition of the first leachates (L1), which display high $^{55}Mn/^{52}Cr$ ratios of about 20 for the EH3 and 35 for the EL3. The first step of the leaching procedure most likely dissolved soluble sulphides such as oldhamite (CaS), niningerite (MgS) and alabandite (MnS). Alabandite and niningerite are diagnostic minerals for distinguishing between the subgroups of enstatite chondrites as they are only observed in EL and EH chondrites, respectively. These sulphide phases therefore contribute to different Mn/Cr for leachates of the EH3 and EL3 chondrites. The shallow slopes contrast with isochrons obtained by other studies on enstatite chondrites (Figure 7). Shukolyukov and Lugmair (2004) leached equilibrated chondrites of petrologic types 4 and 6. Little disturbance is observed in these isochrons compared to those produced with unequilibrated enstatite chondrites from this study and that of Kadlag et al. (2021) (Figure 7). Redistribution of Mn and Cr between mineral phases during metamorphism of enstatite chondrites of types 4 to 6 may have homogenised the primitive chondritic components to provide the meaningful isochrons produced by Shukolyukov and Lugmair (2004). The source of the ill-defined slopes in type 3 EC may represent mixing between different components and could result in discrepancies in the isochron diagram due to chemical and isotopic disequilibrium between components. The scatter may also be attributed to irradiation that produces excesses in $\varepsilon^{53}Cr$ as discussed in the previous section. Given the scattering in the data and the impossibility of sorting leachates objectively, temporal constraints cannot be determined for the three type 3 meteorites investigated using the Mn-Cr systematics.

4.3 Chromium nucleosynthetic heterogeneities in ordinary chondrites

4.3.1 Nucleosynthetic components inferred from the leachates

The magnitude of isotopic anomalies in leachates can be related to (1) the magnitude of deviation of the composition of the anomalous component from the bulk chondrite composition; (2) the relative Cr contribution of the anomalous component in each leachate, i.e. the degree to which the anomalous component is diluted in "normal" Cr; (3) the presence of multiple components with anomalous compositions. These effects need to be carefully considered before drawing conclusions on the composition of the endmembers from leachates and components of chondrites. Leaching experiments on ordinary chondrites of the L subgroup were reported by Wang et al. (2011) and Qin et al. (2011a). At first sight, this

work does not appear to agree with these previous studies (Figure 5). Due to different leaching procedures (results for 4 to 7 steps), leachate steps do not correspond to the same minerals dissolved. However, the three studies complement each other. The present study allows for a more detailed description of the easily soluble minerals such as sulphides. L1 and L2 show the existence of a component characterised by an $\varepsilon^{54}Cr$ of ~-1.5, which is mixed with other components in Semarkona and Queen Alexandra Range (QUE) 97008 (Wang et al., 2011; Qin et al., 2011a, respectively), resulting in stronger negative anomalies for $\varepsilon^{54}Cr$. Components dissolved in L3 and L4, with negative $\varepsilon^{54}Cr$ ~-6, appear to correspond to the first leachates steps of other studies. The majority of Cr (87 %) in NWA 8007 is hosted in L5 and L6, impeding accurate characterisation of the anomalous components. The procedure of Wang et al. (2011) provides constraints on the refractory mineral phases and shows the existence of positive $\varepsilon^{54}Cr$ anomalies (4.4 ± 0.5 and 3.5 ± 0.3) obtained in leachates with 6 M HCl at 40 °C and 80 °C. The low magnitude of $\varepsilon^{54}Cr$ anomalies in L5 and L6 of NWA 8007 in our study, close to the terrestrial composition, is consistent with the study of Wang et al. (2011) and Qin et al. (2011a). The last leachate (a mixture of concentrated HF and HNO_3) reported by Qin et al. (2011a) on QUE 97008 displays a strong negative anomaly but with a low precision (-4.4 ± 2.3). The discrepancy between the leachates' $\varepsilon^{54}Cr$ and the bulk composition led Qin et al. (2011a) to calculate a theoretical composition of the last leachate of + 0.77 $\varepsilon^{54}Cr$ that agrees with our study on NWA 8007 and the study of Wang et al. (2011) on Semarkona.

Three main components are found using leachates of unequilibrated OC, (1) a component with positive $\varepsilon^{54}Cr$ anomalies, (2) a component with negative $\varepsilon^{54}Cr$ anomalies and (3) a component with a "normal" composition, close to the composition of the bulk meteorite. The first component, identified by Wang et al. (2011), is sampled in 6 M HCl leachates L4 and L5 of Semarkona (Wang et al., 2011) with $\varepsilon^{54}Cr$ of 4.4 ± 0.5 and 3.5 ± 0.3, respectively. This component is also present in leachates of L5 and L6 of NWA 8007 and potentially in L6 of Semarkona. The lower intensity of the anomalies is likely related to a mixture of this component with one or both remaining components. This component may be related to the very strong positive $\varepsilon^{54}Cr$ anomalies, more than 100 ε units, also sampled in 6 M HCl leachates in carbonaceous chondrites (e.g. Rotaru et al., 1992; Podosek et al., 1997). The second component is determined with the negative $\varepsilon^{54}Cr$ compositions measured in L3 and L4 in NWA 8007 and the first leachates of Semarkona and QUE 97008. It may be related to a similar component which has also been reported in studies on leachates and separates of carbonaceous chondrites (Yamakawa and Yin, 2014; Göpel et al., 2015; Kadlag et al., 2019). The $\varepsilon^{54}Cr$ composition of the leachates L1 and L2 of NWA 8007 likely represents a mixture between this component with negative $\varepsilon^{54}Cr$ and normal Cr. The last component constitutes the largest Cr reservoir and displays a Cr isotope composition similar to that of the bulk meteorite. The leachates representing the largest Cr budget systematically exhibit the lowest anomalies (Figure 5).

4.3.2 Nature of anomalous components

The homogeneity of the nucleosynthetic Cr composition in chondrules (Schneider et al., 2020; Williams et al., 2020) suggests that carriers of anomalous compositions are hosted in the matrix of ordinary chondrites. Carrier phases of $\varepsilon^{54}Cr$ anomalies are difficult to identify from leachate compositions, but some

conclusions can nonetheless be drawn. Many types of presolar grains have been identified and are usually refractory minerals such as nano-diamonds, silicon carbides, graphite, oxides but also include silicates. Nano-diamonds and silicates are the most abundant presolar grains in the most primitive chondrites, with 1400 ppm and 200 ppm, respectively (Zinner et al., 2014; Floss and Haenecour, 2016). Few presolar grains have been found to contain Cr and are predominantly oxides containing varying amounts of Al and Mg (Zinner et al., 2005; Dauphas et al., 2010; Qin et al., 2011b; Nittler et al., 2018). Presolar silicon carbide grains host Cr in small amounts and their isotope composition is slightly different from the composition of the Solar System and does not match the modelled *s*-process that occurs in AGB stars producing SiC (Levine et al., 2009; Savina et al., 2010). These authors suggested that the Cr isotope composition is inherited from the starting materials of the AGB stars rather than produced in the AGB stars themselves. However, SiC grains are unlikely to be a significant presolar carrier of Cr because they would yield larger anomalies in the very last leachates, which is what is observed for Nd and Sm for instance (Frossard et al., 2022). Some presolar silicates may contain trace amounts of Cr (below 1 at. %) (Nguyen et al., 2016). The Cr content of presolar silicates has not been studied in detail but is often inferred from ^{52}Cr measurements to correct ^{54}Cr isobaric interference on ^{54}Fe in Fe isotope analyses. These measurements suggest that the few grains for which Cr has been identified as traces display solar $^{54}Cr/^{52}Cr$ ratios. The only presolar grains carrying anomalous nucleosynthetic compositions of Cr are oxides (Dauphas et al., 2010; Qin et al., 2011b; Nittler et al., 2018). These grains are characterised by high $^{54}Cr/^{52}Cr$ ratios, near solar $^{53}Cr/^{52}Cr$ and $^{50}Cr/^{52}Cr$ ratios, the former often depleted and the latter often enriched compared to the solar composition. Contrary to presolar grain compositions, our data is corrected for mass fractionation using a fixed $^{50}Cr/^{52}Cr$ ratio. Therefore, excesses in the $^{50}Cr/^{52}Cr$ ratio would result in even larger excesses in $^{54}Cr/^{52}Cr$ and $^{53}Cr/^{52}Cr$ normalised ratios compared to the solar composition.

The first component displaying high $\varepsilon^{54}Cr$ in the leachates has been proposed to arise from nanometer-sized oxides enriched in ^{54}Cr (Podosek et al., 1997; Dauphas et al., 2010; Qin et al., 2011b; Wang et al., 2011; Nittler et al., 2018). The leachates obtained with 6 M HCl in the least thermally processed CC chondrites display a higher magnitude of $\varepsilon^{54}Cr$ anomalies, reaching up to 211 $\varepsilon^{54}Cr$ (Podosek et al., 1997), compared to the leachates of ordinary chondrites. This difference may be due to several processes. First, this may be related to dilution in "normal" Cr due to the relative proportions of components and the magnitude of their nucleosynthetic anomalies. Indeed, in various chondrite types minerals dissolved at each step of the leaching procedure contain different Cr contents. Most minerals display a relatively homogeneous Cr isotope composition in comparison to leachates as evidenced by the relatively homogeneous Cr isotope composition of chondrules (Schneider et al., 2020; Williams et al., 2020) that correspond to 60 to 80 % in volume of ordinary chondrites (Brearley and Jones, 1998). Therefore, "normal" Cr that is dissolved in each leachate step dilutes the isotopic anomalies carried by minor anomalous phases, decreasing their magnitude.

The nature of the second component with negative $\varepsilon^{54}Cr$ in the leachates is unknown but is not hosted in refractory phases in ordinary chondrites because they are obtained by dissolving minerals in relatively mild acids up to 6 M HCl at 60 °C. The results obtained from the leaching of NWA 8007 in this study suggest that the component with negative $\varepsilon^{54}Cr$ sampled in L3 and L4 does not correspond to the most

soluble phases such as phosphates or sulphides, which are dissolved in the first and second steps (0.5 M acetic acid and 0.5 M HNO_3 at room temperature). The results obtained with the procedures applied to Semarkona and QUE 97008 suggest otherwise because the most negative anomalies were obtained in the first leachates obtained with 8.5 or 8.7 M acetic acid that likely include the signatures measured in L1, L2 and L3 of NWA 8007. Minerals dissolved in the leaching steps 3-4 most likely include metal (mostly step 3) and silicates, particularly plagioclase based on REE compositions (see Frossard et al., 2022 for trace element data). Plagioclase contains very little Cr, in contrast to metal. However, negative ε^{54}Cr anomalies are unlikely to be hosted in the metal as they are slightly stronger in L4 at which point metal was already leached out. This component may trace subtle negative ε^{54}Cr compositions hosted in presolar silicates that are the only presolar grain other than oxides that may host Cr. This hypothesis fits well with the likelihood of presolar silicates to be leached in the steps 3 and 4 where negative ε^{54}Cr compositions are obtained. More work is required to identify this component and Cr isotope compositions of presolar silicates would be very interesting in that regard.

4.4 Reduced conditions as the origin of enstatite chondrites ε^{54}Cr homogeneity

The magnitude of the Cr nucleosynthetic anomalies of enstatite chondrite leachates is very low compared to that of ordinary chondrites (Figures 4 and 5) but are very similar despite the two chondrites belonging to two different subgroups, EL and EH. This is surprising as the same leachates from enstatite chondrites display large Nd and Sm nucleosynthetic anomalies (Frossard et al., 2022). Unequilibrated enstatite chondrite falls are rare, and terrestrial weathering could affect Cr isotope compositions. However, we deem this hypothesis unlikely as leachates from the EH3 fall Kota-Kota (Kadlag et al., 2021) display essentially the same isotope composition as the two finds from the Sahara and Antarctica used in this study. Moreover, Nd and Sm isotope compositions of the same samples are not affected by weathering, whereas these elements are more susceptible than Cr to terrestrial contamination as the continental crust is enriched in light rare-earth elements (Frossard et al., 2022).

In enstatite chondrites, Cr is mainly hosted in the L3 leaching step (between 67 % and 69 % of the total Cr of all leachates). This means that if anomalous phases were present, there would be sufficiently low Cr in the leachates other than L3 for these to be identified. The magnitude of the anomalies is below 0.6 ε units in enstatite chondrites whereas it reaches several ε units in ordinary chondrites and up to 130 ε units in the CI carbonaceous chondrite Orgueil for similar Cr contents (Rotaru et al., 1992). Hence, similar carriers present in fractions other than leachate 3 should be easily identified. The results for Sahara 97158 and PCA 91020 from this study agree with the results of a leaching experiment carried out on the EH3 chondrite Kota-Kota by Kadlag et al. (2021) as well as 6 M HCl leachates of insoluble organic matter-rich residues of EC obtained after CsF-HF digestion from Qin et al. (2010).

The small range of variation in enstatite chondrite leachates that is observed is most likely related to irradiation as discussed by Kadlag et al. (2021) and above. The origin of this homogeneity probably arises from the reducing conditions in which enstatite chondrites formed, very distinct from that of other chondrite groups. Enstatite chondrites have an oxygen fugacity at least two log units below the iron-wüstite

buffer (ΔIW-2), and most likely between ΔIW-4 and ΔIW-6 with a high sulphur fugacity (e.g. Brett and Sato, 1974; McKeown et al., 2014; Lin, 2022; Hammouda et al., 2022). Sahara 97158 and PCA 91020 have experienced higher temperatures of metamorphism relative to type 3 ordinary chondrites, possibly up to 640 °C based on noble gas studies in other types 3 and 4 EC (Huss and Lewis, 1994). Their textures and the chemical composition of the minerals remain however unequilibrated (Weisberg and Kimura, 2012). Interestingly, despite having similar peak temperatures compared to Allende (530-600 °C) (Huss and Lewis, 1994; Busemann et al., 2007), leachates of enstatite chondrites display a much smaller range of ε^{54}Cr of 0.4 compared to leachates of Allende displaying a range of 2.0 ε units. Enstatite chondrites contain very small amounts of oxide minerals and most silicates are highly reduced with the exception of some rare crystals in the matrix (Rambaldi et al., 1984). Oxides are not stable under such oxygen and sulphur fugacities. Given that the only presolar Cr carrier identified so far is an oxide (Dauphas et al., 2010; Qin et al., 2011b; Nittler et al., 2018), it is unlikely that it survived in this environment. This is also supported by the very limited amount of presolar oxides found in enstatite chondrites compared to other classes of chondrites (Lin et al., 2002). The homogeneity in ε^{54}Cr compositions of enstatite chondrite leachates is evidence that the main presolar Cr carriers are relatively oxidised and that presolar silicon carbide is not a significant contributor of anomalous Cr because it is more resistant to thermal metamorphism under reducing environments than oxidising conditions (Huss and Lewis, 1994).

4.5 Effects of parent body processing on the Cr isotope compositions of leachates

Thermal metamorphism and aqueous alteration can induce the redistribution of elements and blur the nucleosynthetic information hosted in presolar carriers (Zinner, 2014; Davidson et al., 2014; Floss and Haenecour, 2016; Riebe et al., 2020; Yokoyama et al., 2023). The isotope composition of the leachates is therefore affected by these processes. The redistribution of the anomalous components is a significant issue for Cr isotope compositions of the leachates of primitive chondrites because of disturbances of the Mn-Cr systematics that affect ε^{53}Cr compositions. These processes render the identification of anomalous components difficult because the composition of the leachates may not represent the initial component or carrier but rather that of the secondary minerals that formed through parent body processing. The comparison of the leachates' Cr isotope composition is also complicated between the chondrite groups as they have different mineralogy and experienced different degrees of parent body processing under different conditions.

Thermal metamorphism significantly affects the composition of leachates and tends to destroy presolar phases. The ordinary chondrites that were processed in this study and studies of Qin et al. (2011a) and Wang et al. (2011) range from petrologic types 3.0 to 3.2 according to the scale determined using Cr content in olivine (Grossman and Brearley, 2005) with peak temperatures likely below 300 °C. The peak temperature of Semarkona has been estimated between 220 and 260 °C (Alexander et al., 1989; Busemann et al., 2007). A comparison of the Cr isotope compositions of the leachates of the three OC does not indicate a clear link with the petrologic type (Figure 8). In the carbonaceous groups, the observation of leachates displaying large positive ε^{53}Cr compositions is diagnostic of the effect of thermal metamorphism (Figure 9). Excesses in

476 ε^{53}Cr are systematically observed in CC having experienced significant thermal metamorphism such as the
477 oxidised CV3 chondrite Allende, CO chondrites Lancé and Felix and CK chondrite Karoonda (Rotaru et
478 al., 1992; Trinquier et al., 2007). The degree of maturity of the organic matter in these chondrites suggests
479 that they have a petrologic sub-type above 3.6 and experienced peak temperatures between 480 °C (Lancé)
480 and 600 °C (Allende) (Bonal et al., 2006, 2007; Busemann et al., 2007), therefore higher than the type 3 OC
481 studied here and in the literature. The decreasing range of variation of ε^{54}Cr in leachates of each meteorite
482 is also related to thermal metamorphism but is more difficult to compare between chondrite groups because
483 of their different mineralogy, i.e. Cr not being distributed in the same phases.
484 Aqueous alteration predominantly affects carbonaceous chondrites and induces substantial excesses in
485 ^{53}Cr found in leachates of CI chondrites and the ungrouped C2 chondrite Tagish Lake (Figure 9). These
486 signatures are evidence for in situ decay of ^{53}Mn in Mn-rich phases, most likely carbonates (Endreß and
487 Bischoff, 1996; Rotaru et al., 1992; Trinquier et al., 2007; Yamakawa and Yin, 2014; Göpel et al., 2015). On
488 the other hand, unequilibrated ordinary chondrites have also experienced aqueous alteration (Alexander et
489 al., 1989; Grossman et al., 2000; Dobrică and Brearley, 2020), but no excess in ε^{53}Cr can indubitably
490 attributed to aqueous alteration in the leachates of OC. In conclusion, the Cr isotope composition of
491 leachates of chondrites may not reflect primitive compositions because host phases are modified by thermal
492 processing and aqueous alteration under various redox conditions.
493 Presolar grains are variably affected by parent body processing. The abundance of presolar nano-
494 diamonds and silicates may be used as an indicator of the degree of processing of unequilibrated chondrites
495 (e.g. Huss and Lewis, 1994; Zinner, 2014). Among the potential presolar carriers of Cr, oxides are relatively
496 stable during aqueous alteration, whereas silicates are very easily altered (Nguyen et al., 2007). Indeed, the
497 silicate/oxide ratio is particularly useful in determining the degree of aqueous alteration because the most
498 primitive chondrites such as CR3, interplanetary dust particles (IDP) and AGB stars all display a very similar
499 presolar silicate/oxide ratio (Floss and Stadermann, 2009; Leitner et al., 2012; Floss and Haenecour, 2016).
500 Heterogeneities in both ^{53}Cr and ^{54}Cr anomalies of different Ryugu samples (returned by the Hayabusa2
501 spacecraft) that are closely related to CI chondrites are also linked to secondary parent-body processes
502 (Yokoyama et al., 2023). Extensive aqueous alteration and formation of Cr-bearing secondary minerals could
503 explain the redistribution of Cr and associated isotopic anomalies among samples. Ordinary chondrites
504 Semarkona and QUE 97008 contain similar abundances of presolar silicates and oxides (O-anomalous
505 presolar grains), 151 and 125 ppm, respectively (Barosch et al., 2022; Floss and Haenecour, 2016). This is
506 in good agreement with the range of the Cr isotope anomalies identified in the leachates of these two
507 chondrites. Despite their resistance to aqueous alteration, presolar oxides are prone to be destroyed by
508 thermal metamorphism. Their destruction could in part explain the reduced range of ε^{54}Cr observed in the
509 leachates of type 3.00 to 3.2 OC compared to leachates of CI and CM2 chondrites.

510 ### 4.6 Constraints on the origin of nucleosynthetic variations in chondrites

511 The Cr isotope composition of leachates indicates that there are at least 3 major endmembers as
512 detailed above. The most anomalous endmember is ^{54}Cr-rich presolar oxides. The negative endmember may

513 be presolar silicates or another phase that appears complementary to ^{54}Cr-rich oxides. The leachates of CM2
514 chondrites are particularly interesting in defining the principal endmembers affecting the nucleosynthetic
515 variations between meteorite groups because the aqueous alteration did not produce large excesses in ε^{53}Cr
516 while preserving the presolar nano-oxides rich in ^{54}Cr. The negative endmember observed in ordinary
517 chondrites is, however, likely to have been homogeneised. Presolar silicates, for instance, occur in much
518 lower concentrations in aqueously altered CM2 chondrites and have been replaced by secondary
519 phyllosilicates (Floss and Haenecour, 2016; Leitner et al., 2020). The Cr isotope compositions of leachates
520 of CM2 chondrites align in a ε^{53}Cr vs. ε^{54}Cr diagram, with a slope of -47 ± 11 (model 1 of IsoplotR,
521 Vermeesch, 2018) with little spread in ε^{53}Cr that is linked to thermal processing and high degrees of aqueous
522 alteration. This trend can be explained by the mixing of two endmembers, one with a high ε^{54}Cr and small
523 negative ε^{53}Cr and the other with low ε^{54}Cr and slightly positive ε^{53}Cr (Figure 10). Other studies also
524 identified the importance of these two endmembers (Yamakawa and Yin, 2014; Göpel et al., 2015). The
525 negative endmember is essentially complementary to the ^{54}Cr-rich endmember that carries the most
526 anomalous composition.
527 Other components exist in chondrites but are not predominant in terms of budget. Yamakawa and
528 Yin (2014) provide a detailed discussion on the contributors of Cr isotope anomalies in chondrites. For
529 instance, CAIs display different compositions to bulk chondrites and plot close to the trend of CM2
530 leachates (Figure 10). The Mn/Cr ratios are fractionated in the different groups of CAIs and produce
531 variable radiogenic ε^{53}Cr. Once corrected for the radiogenic ingrowth, CAIs are slightly offset from the
532 CM2 leachate trend and spread with a different slope (Torrano et al., 2023) (Figure 10). The FUN
533 (Fractionated Unknown Nuclear) refractory inclusions are other rare components of chondrites that display
534 exotic Cr isotope compositions (Papanastassiou, 1986). Overall, refractory inclusions do not influence
535 substantially the Cr isotope composition of leachates because of their relatively low Cr content (350-1250
536 ppm, compared to 3650 ppm in bulk CV3, Stracke et al., 2012).
537 The origin of the distinct Cr isotopic compositions of bulk chondrite meteorites is debated but
538 leachates provide valuable information in that regard. The bulk composition of ordinary chondrites is
539 slightly depleted in ε^{54}Cr (-0.2 ε^{54}Cr) compared to enstatite chondrites that display an Earth-like signature
540 (ε^{54}Cr=0) and to carbonaceous chondrites that display positive ε^{54}Cr between +0.5 and +1.5 (e.g. Trinquier
541 et al., 2007) (Figure 11). The predominance of the signature of an endmember with high ε^{54}Cr and near
542 normal ε^{53}Cr and its complementary endmember suggests that bulk compositions reflect the heterogeneous
543 distribution of ^{54}Cr-rich presolar oxides in the protoplanetary disc. Carbonaceous chondrites appear to be
544 enriched in this endmember relative to non-carbonaceous chondrites (Figure 11). The mechanisms to
545 produce this heterogeneous distribution of presolar carriers of Cr could involve preferential destruction in
546 the protoplanetary disc of carriers of ε^{54}Cr anomalies, the incorporation of carriers from infall of the nebular
547 cloud or physical sorting of materials in the protoplanetary disc (e.g. Trinquier et al., 2009; Van Kooten et
548 al., 2016; Steele et al., 2012).

5. Conclusion

The Cr isotope compositions of the leachates of the ordinary chondrite NWA 8007 (L3.2) and the enstatite chondrites PCA 91020 (EL3) and Sahara 97158 (EH3) were measured from the same solutions that were analysed for their Nd and Sm isotope compositions (Frossard et al., 2022). Leachates from the ordinary chondrite display large variations in both ε^{53}Cr and ε^{54}Cr, whereas Nd and Sm anomalies were barely resolved. In contrast, leachates of the enstatite chondrites of the EL and EH groups display significant variations for ε^{53}Cr and only small variations for ε^{54}Cr. Despite variations on the ε^{53}Cr bearing radiogenic ingrowths, the mismatch with Mn/Cr ratios rules out obtaining any temporal information. Stark differences are observed between nucleosynthetic ε^{54}Cr anomalies in leachates of ordinary and enstatite chondrites, confirming previous studies on other samples. Leachates of the ordinary chondrite exhibit large nucleosynthetic anomalies from -6.68 to +0.84 ε^{54}Cr. Examination of leachates of ordinary chondrites from the literature and their respective procedures shows that there are at least 2 different nucleosynthetic components. Elevated ε^{54}Cr compositions in leachates, mostly obtained with 6 M HCl, may correspond to ^{54}Cr-rich presolar oxides identified in carbonaceous chondrites. The second component with negative ε^{54}Cr is dissolved in relatively mild acids and could correspond to presolar silicate. Leachates of enstatite chondrites show very little ε^{54}Cr variation. The presolar heritage for Cr of these chondrites has been erased and ε^{54}Cr composition of leachates has been homogenised. Small variations in ε^{53}Cr and ε^{54}Cr can be attributed to irradiation by cosmic rays. The leachates of the unequilibrated chondrites do not carry primordial compositions and components inferred from them cannot be readily assimilated to nucleosynthetic endmembers carried by presolar grains. Thermal metamorphism and aqueous alteration had a significant effect on Cr isotope compositions in chondrites. Comparing leachates of various types of chondrites, we show that mild thermal metamorphism in unequilibrated (type 3) chondrites particularly affects the Cr isotope composition of leachates and Cr-bearing presolar grains. Redox conditions played an important role in the destruction of presolar grains and redistribution of their anomalous Cr in other minerals. The case of enstatite chondrites is particularly interesting because of their homogeneous ε^{54}Cr composition. This homogeneity suggests that Cr presolar carriers are not stable under the reducing conditions in which enstatite chondrites formed. One nucleosynthetic endmember with high ε^{54}Cr and slightly negative ε^{53}Cr contributes to most of the Cr isotope variation in the chondrites. Its heterogeneous distribution in the protoplanetary disc likely produced the variation in the ε^{54}Cr composition of bulk meteorites, with minor contribution of other components such as CAIs. Our study shows that leaching experiments in unequilibrated ordinary and enstatite chondrites hold valuable information on the carriers of nucleosynthetic anomalies and should be more extensively studied for various other elements.

Acknowledgements: We would like to thank Conel Alexander, two anonymous reviewers and the AE Vinciane Debaille for thorough and complementary reviews that improved and clarified the manuscript. We thank Delphine Auclair and Jean-Luc Piro for assistance on the TIMS and Q-ICP-MS, respectively and Chantal Bosq for her management of the clean lab facilities. PF thanks Précillia Morino and Miriam

Rüfenacht for discussion and Maria Schönbächler for allowing him to finalise this study while at ETH Zürich. We thank the Antarctic Meteorite Collection for providing us with the meteorite PCA 91020,88. US Antarctic meteorite samples are recovered by the Antarctic Search for Meteorites (ANSMET) program which has been funded by NSF and NASA, and characterised and curated by the Department of Mineral Sciences of the Smithsonian Institution and Astromaterials Curation Office at NASA Johnson Space Center. This project has received funding from the European Research Council (ERC) under the European Union's Horizon 2020 research and innovation program (Grant Agreement No. 6822778) to MB, from the Canada Foundation for Innovation (33353), NSERC Discovery Grant (06310-2014) and Canada Research Chairs programs (950-229061) to AB. This is Laboratory of Excellence ClerVolc contribution n°XX.

Data availability: Data are available through the Astromaterials Data Repository (AstroRepo) at https://doi.org/10.26022/IEDA/112944.

References

Alexander C. M. O., Barber D. J. and Hutchison R. (1989) The microstructure of Semarkona and Bishunpur. Geochimica et Cosmochimica Acta 53, 3045–3057.

Alibert Y., Venturini J., Helled R., Ataiee S., Burn R., Senecal L., Benz W., Mayer L., Mordasini C., Quanz S. P. and Schönbächler M. (2018) The formation of Jupiter by hybrid pebble–planetesimal accretion. Nat. Astron. 2, 873–877.

Barosch J., Nittler L. R., Wang J., Dobrică E., Brearley A. J., Hezel D. C. and Alexander C. M. O. (2022) Presolar O- and C-anomalous grains in unequilibrated ordinary chondrite matrices. Geochim. Cosmochim. Acta 335, 169–182.

Bermingham K. R., Füri E., Lodders K. and Marty B. (2020) The NC-CC Isotope Dichotomy: Implications for the Chemical and Isotopic Evolution of the Early Solar System. Space Sci. Rev. 216, 133.

Birck J. L. and Lugmair G. W. (1988) Nickel and chromium isotopes in Allende inclusions. Earth and Planetary Science Letters 90, 131–143.

Birck J. L., Rotaru M. and Allègre C. J. (1999) ^{53}Mn-^{53}Cr evolution of the early solar system. Geochim. Cosmochim. Acta 63, 4111–4117.

Birck J.-L. and Allègre C. J. (1985) Evidence for the presence of ^{53}Mn in the early solar system. Geophys. Res. Lett. 12, 745–748.

Bonal L., Bourot-Denise M., Quirico E., Montagnac G. and Lewin E. (2007) Organic matter and metamorphic history of CO chondrites. Geochim. Cosmochim. Acta 71, 1605–1623.

Bonal L., Quirico E., Bourot-Denise M. and Montagnac G. (2006) Determination of the petrologic type of CV3 chondrites by Raman spectroscopy of included organic matter. Geochim. Cosmochim. Acta 70, 1849–1863.

Bonnand P. and Halliday A. N. (2018) Oxidized conditions in iron meteorite parent bodies. Nat. Geosci. 11, 401–404.

Bonnand P., Parkinson I. J., James R. H., Karjalainen A.-M. and Fehr M. A. (2011) Accurate and precise determination of stable Cr isotope compositions in carbonates by double spike MC-ICP-MS. J. Anal. At. Spectrom. 26, 528–535.

Bonnand P., Williams H. M., Parkinson I. J., Wood B. J. and Halliday A. N. (2016) Stable chromium isotopic composition of meteorites and metal–silicate experiments: Implications for fractionation during core formation. Earth Planet. Sci. Lett. 435, 14–21.

Bourdon B. and Fitoussi C. (2020) Isotope Fractionation during Condensation and Evaporation during Planet Formation Processes. ACS Earth Space Chem. 4, 1408–1423.

Brasser R. and Mojzsis S. J. (2020) The partitioning of the inner and outer Solar System by a structured protoplanetary disk. Nat. Astron. 4, 492–499.

Brearley A. J. and Jones R. H. (1998) Chondritic meteorites. Rev. Min. Geochem. 36, 3–01.

Brearley A. J. (2014) Nebular Versus Parent Body Processing. In Treatise on Geochemistry Elsevier. pp. 309–334.

Brett R. and Sato M. (1984) Intrinsic oxygen fugacity measurements on seven chondrites, a pallasite, and a tektite and the redox state of meteorite parent bodies. Geochim. Cosmochim. Acta 48, 111–120.

Busemann H., Alexander M. O. and Nittler L. R. (2007) Characterization of insoluble organic matter in primitive meteorites by microRaman spectroscopy. Meteorit. Planet. Sci. 42, 1387–1416.

Clayton D. (2003) Handbook of Isotopes in the Cosmos., Cambridge University Press, Cambridge, UK.

Cornet M., Fitoussi C., Bourdon B. and Pili E. (2022) Determination of chromium isotopic composition in various geological material by thermal ionization mass spectrometry. Int. J. Mass Spectrom. 480, 116897.

Dauphas N., Chen J. H., Zhang J., Papanastassiou D. A., Davis A. M. and Travaglio C. (2014) Calcium-48 isotopic anomalies in bulk chondrites and achondrites: Evidence for a uniform isotopic reservoir in the inner protoplanetary disk. Earth Planet. Sci. Lett. 407, 96–108.

Dauphas N., Remusat L., Chen J. H., Roskosz M., Papanastassiou D. A., Stodolna J., Guan Y., Ma C. and Eiler J. M. (2010) Neutron-rich chromium isotope anomalies in supernova nanoparticles. ApJ 720, 1577–1591.

Davidson J., Busemann H., Nittler L. R., Alexander C. M. O., Orthous-Daunay F.-R., Franchi I. A. and Hoppe P. (2014) Abundances of presolar silicon carbide grains in primitive meteorites determined by NanoSIMS. Geochim. Cosmochim. Acta 139, 248–266.

Dobrică E. and Brearley A. J. (2020) Amorphous silicates in the matrix of Semarkona: The first evidence for the localized preservation of pristine matrix materials in the most unequilibrated ordinary chondrites. Meteorit. Planet. Sci. 55, 649–668.

Endreß M. and Bischoff A. (1996) Carbonates in CI chondrites: Clues to parent body evolution. Geochim. Cosmochim. Acta 60, 489–507.

Floss C. and Stadermann F. (2009) Auger Nanoprobe analysis of presolar ferromagnesian silicate grains from primitive CR chondrites QUE 99177 and MET 00426. Geochim. Cosmochim. Acta 73, 2415–2440.

Floss C. and Haenecour P. (2016) Presolar silicate grains: Abundances, isotopic and elemental compositions, and the effects of secondary processing. Geochem. J. 50, 3–25.

Fricke G., Heilig K., "Nuclear Charge Radii" in Landolt-Börnstein - Group I: Elementary Particles, Nuclei and Atoms, Schopper, H., Ed. (Springer, 2004), vol. 20.

Frossard P., Israel C., Bouvier A. and Boyet M. (2022) Earth's composition was modified by collisional erosion. Science 377, 1529–1532.

Fujii T., Moynier F. and Albarede F. (2006) Nuclear field vs. nucleosynthetic effects as cause of isotopic anomalies in the early Solar System. Earth Planet. Sci. Lett. 247, 1–9.

Fujiya W., Sugiura N., Hotta H., Ichimura K. and Sano Y. (2012) Evidence for the late formation of hydrous asteroids from young meteoritic carbonates. Nat. Commun. 3, 627.

Glavin D. P., Kubny A., Jagoutz E. and Lugmair G. W. (2004) Mn-Cr isotope systematics of the D'Orbigny angrite. Meteorit. Planet. Sci. 39, 693–700.

Göpel C., Birck J.-L., Galy A., Barrat J.-A. and Zanda B. (2015) Mn–Cr systematics in primitive meteorites: Insights from mineral separation and partial dissolution. Geochim. Cosmochim. Acta 156, 1–24.

Grossman J. N., Alexander C. M. O., Wang J. and Brearley A. J. (2000) Bleached chondrules: Evidence for widespread aqueous processes on the parent asteroids of ordinary chondrites. Meteorit. Planet. Sci. 35, 467–486.

Grossman J. N. and Brearley A. J. (2005) The onset of metamorphism in ordinary and carbonaceous chondrites. Meteorit. Planet. Sci. 40, 87–122.

Hammouda T., Boyet M., Frossard P. and Cartier C. (2022) The message of oldhamites from enstatite chondrites. Prog. Earth Planet. Sci. 9, 13.

Hibiya Y., Iizuka T., Yamashita K., Yoneda S. and Yamakawa A. (2019) Sequential Chemical Separation of Cr and Ti from a Single Digest for High-Precision Isotope Measurements of Planetary Materials. Geostand. Geoanal. Res. 43, 133–145.

Huss G. R. and Lewis R. S. (1994) Noble gases in presolar diamonds II: Component abundances reflect thermal processing. Meteoritics 29, 811–829.

Jenniskens P., Fries M. D., Yin Q.-Z., Zolensky M., Krot A. N., Sandford S. A., Sears D., Beauford R., Ebel D. S., Friedrich J. M., Nagashima K., Wimpenny J., Yamakawa A., Nishiizumi K., Hamajima Y., Caffee M. W., Welten K. C., Laubenstein M., Davis A. M., Simon S. B., Heck P. R., Young E. D., Kohl I. E., Thiemens M. H., Nunn M. H., Mikouchi T., Hagiya K., Ohsumi K., Cahill T. A., Lawton J. A., Barnes D., Steele A., Rochette P., Verosub K. L., Gattacceca J., Cooper G., Glavin D. P., Burton A. S., Dworkin J. P., Elsila J. E., Pizzarello S., Ogliore R., Schmitt-Kopplin P., Harir M., Hertkorn N., Verchovsky A., Grady M., Nagao K., Okazaki R., Takechi H., Hiroi T., Smith K., Silber E. A., Brown P. G., Albers J., Klotz D., Hankey M.,

695 Matson R., Fries J. A., Walker R. J., Puchtel I., Lee C.-T. A., Erdman M. E., Eppich G. R., Roeske S.,
696 Gabelica Z., Lerche M., Nuevo M., Girten B., Worden S. P., and (the Sutter's Mill Meteorite Consortium)
697 (2012) Radar-Enabled Recovery of the Sutter's Mill Meteorite, a Carbonaceous Chondrite Regolith Breccia.
698 Science 338, 1583–1587.
699 Kadlag Y., Becker H. and Harbott A. (2019) Cr isotopes in physically separated components of the Allende
700 CV 3 and Murchison CM 2 chondrites: Implications for isotopic heterogeneity in the solar nebula and parent
701 body processes. Meteorit. Planet. Sci. 54, 2116–2131.
702 Kadlag Y., Hirtz J., Becker H., Leya I. and Mezger K. (2021) Early solar irradiation as a source of the inner
703 solar system chromium isotopic heterogeneity. Meteorit. Planet. Sci. 56, 2083–2102.
704 Kruijer T. S., Burkhardt C., Budde G. and Kleine T. (2017) Age of Jupiter inferred from the distinct genetics
705 and formation times of meteorites. Proc. Natl. Acad. Sci. U.S.A. 114, 6712–6716.
706 Langbroek M., Jenniskens P., Kriegsman L. M., Nieuwenhuis H., De Kort N., Kuiper J., Van Westrenen
707 W., Zolensky M. E., Ziegler K., Yin Q.-Z., Sanborn M. E., Wimpenny J., Yamakawa A., De Vet S. J., Meier
708 M. M. M., Welten K. C., Nishiizumi K., Caffee M. W., Burton A. S., Dworkin J. P., Glavin D. P., Wu Q.,
709 Zare R. N., Ruf A., Harir M., Schmitt-Kopplin P., and The Diepenveen Meteorite Consortium (2019) The
710 CM carbonaceous chondrite regolith Diepenveen. Meteorit. Planet. Sci. 54, 1431–1461.
711 de Leuw S., Rubin A. E., Schmitt A. K. and Wasson J. T. (2009) ^{53}Mn–^{53}Cr systematics of carbonates in CM
712 chondrites: Implications for the timing and duration of aqueous alteration. Geochim. Cosmochim. Acta 73,
713 7433–7442.
714 Larsen K. K., Wielandt D., Schiller M. and Bizzarro M. (2016) Chromatographic speciation of Cr(III)-
715 species, inter-species equilibrium isotope fractionation and improved chemical purification strategies for
716 high-precision isotope analysis. J. Chromatogr. A 1443, 162–174.
717 Leitner J., Kodolányi J., Hoppe P. and Floss C. (2012) Laboratory analysis of presolar silicate stardust from
718 a nova. ApJ 754, L41.
719 Leitner J., Metzler K., Vollmer C., Floss C., Haenecour P., Kodolányi J., Harries D. and Hoppe P. (2020)
720 The presolar grain inventory of fine-grained chondrule rims in the Mighei-type (CM) chondrites. Meteorit.
721 Planet. Sci. 55, 1176–1206.
722 Levine J., Savina M. R., Stephan T., Dauphas N., Davis A. M., Knight K. B. and Pellin M. J. (2009)
723 Resonance ionization mass spectrometry for precise measurements of isotope ratios. Int. J. Mass Spectrom.
724 288, 36–43.
725 Leya I., Schönbächler M., Wiechert U., Krähenbühl U. and Halliday A. N. (2008) Titanium isotopes and the
726 radial heterogeneity of the solar system. Earth Planet. Sci. Lett. 266, 233–244.
727 Leya I., Wieler R. and Halliday A. N. (2003) The influence of cosmic-ray production on extinct nuclide
728 systems. Geochim. Cosmochim. Acta 67, 529–541.
729 Lichtenberg T. and Draz J. (2021) Bifurcation of planetary building blocks during Solar System formation.
730 Lin Y. (2022) Enstatite chondrites: condensation and metamorphism under extremely reducing conditions
731 and contributions to the Earth. Prog. Earth Planet. Sci. 9, 28.

Lin Y., Amari S. and Pravdivtseva O. (2002) Presolar Grains from the Qingzhen (EH3) Meteorite. ApJ 575, 257–263.

Liu J., Qin L., Xia J., Carlson R. W., Leya I., Dauphas N. and He Y. (2019) Cosmogenic effects on chromium isotopes in meteorites. Geochim. Cosmochim. Acta 251, 73–86.

Loss R. D., Lugmair G. W., Davis A. M., MacPherson G. J. (1994) Isotopically distinct reservoirs in the solar nebula: Isotope anomalies in Vigarano meteorite inclusions. ApJ 436, L193-L196.

Lugmair G. W. and Shukolyukov A. (1998) Early solar system timescales according to ^{53}Mn-^{53}Cr systematics. Geochim. Cosmochim. Acta 62, 2863–2886.

Ma N., Neumann W., Néri A., Schwarz W. H., Ludwig T., Trieloff M., Klahr H. and Bouvier A. (2022) Early formation of primitive achondrites in an outer region of the protoplanetary disc. Geochem. Persp. Let. 23, 33–37.

McKeown D. A., Buechele A. C., Tappero R., McCoy T. J. and Gardner-Vandy K. G. (2014) X-ray absorption characterization of Cr in forsterite within the MacAlpine Hills 88136 EL3 chondritic meteorite. Am. Min. 99, 190–197.

Mougel B., Moynier F. and Göpel C. (2018) Chromium isotopic homogeneity between the Moon, the Earth, and enstatite chondrites. Earth Planet. Sci. Lett. 481, 1–8.

Moynier F., Yin Q. and Jacobsen B. (2007) Dating the First Stage of Planet Formation. ApJ 671, L181–L183.

Nguyen A. N., Stadermann F. J., Zinner E., Stroud R. M., Alexander C. M. O. and Nittler L. R. (2007) Characterization of presolar silicate and oxide grains in primitive carbonaceous chondrites. ApJ 656, 1223–1240.

Nguyen A. N., Keller L. P. and Messenger S. (2016) Mineralogy of presolar silicate and oxide grains of diverse stellar origins. ApJ 818, 51.

Nittler L. R., Alexander C. M. O., Liu N. and Wang J. (2018) Extremely ^{54}Cr- and ^{50}Ti-rich Presolar Oxide Grains in a Primitive Meteorite: Formation in Rare Types of Supernovae and Implications for the Astrophysical Context of Solar System Birth. ApJ 856, L24.

Papanastassiou D. A. (1986) Chromium isotopic anomalies in the Allende meteorite. ApJ 308, L27.

Pedersen S. G., Schiller M., Connelly J. N. and Bizzarro M. (2019) Testing accretion mechanisms of the H chondrite parent body utilizing nucleosynthetic anomalies. Meteorit. Planet. Sci. 54, 1215–1227.

Petitat M., Birck J.-L., Luu T. H. and Gounelle M. (2011) The chromium isotopic composition of the ungrouped carbonaceous chondrite Tagish Lake. ApJ 736, 23.

Podosek F. A., Ott U., Brannon J. C., Neal C. R., Bernatowicz T. J., Swan P. and Mahan S. E. (1997) Thoroughly anomalous chromium in Orgueil. Meteorit. Planet. Sci. 32, 617–627.

Posner E. S., Ganguly J. and Hervig R. (2016) Diffusion kinetics of Cr in spinel: Experimental studies and implications for ^{53}Mn–^{53}Cr cosmochronology. Geochim. Cosmochim. Acta 175, 20–35.

Qin L., Alexander C. M. O., Carlson R. W., Horan M. F. and Yokoyama T. (2010) Contributors to chromium isotope variation of meteorites. Geochim. Cosmochim. Acta 74, 1122–1145.

769 Qin Liping, Carlson R. W. and Alexander C. M. O. (2011a) Correlated nucleosynthetic isotopic variability
770 in Cr, Sr, Ba, Sm, Nd and Hf in Murchison and QUE 97008. Geochim. Cosmochim. Acta 75, 7806–7828.
771 Qin L., Nittler L. R., Alexander C. M. O., Wang J., Stadermann F. J. and Carlson R. W. (2011b) Extreme
772 ^{54}Cr-rich nano-oxides in the CI chondrite Orgueil – Implication for a late supernova injection into the solar
773 system. Geochim. Cosmochim. Acta 75, 629–644.
774 Quirico E., Bourot-denise M., Robin C., Montagnac G. and Beck P. (2011) A reappraisal of the
775 metamorphic history of EH3 and EL3 enstatite chondrites. Geochim. Cosmochim. Acta 75, 3088–3102.
776 Rambaldi E. R., Housley R. M. and Rajan R. S. (1984) Occurrence of oxidized components in Qingzhen
777 enstatite chondrite. Nature 311, 138–140.
778 Riebe M. E. I., Busemann H., Alexander C. M. O., Nittler L. R., Herd C. D. K., Maden C., Wang J. and
779 Wieler R. (2020) Effects of aqueous alteration on primordial noble gases and presolar SiC in the
780 carbonaceous chondrite Tagish Lake. Meteorit. Planet. Sci. 55, 1257–1280.
781 Rotaru M., Birck J. L. and Allègre C. J. (1992) Clues to early Solar System history from chromium isotopes
782 in carbonaceous chondrites. Nature 358, 465–470.
783 Sanborn M. E., Wimpenny J., Williams C. D., Yamakawa A., Amelin Y., Irving A. J. and Yin Q.-Z. (2019)
784 Carbonaceous achondrites Northwest Africa 6704/6693: Milestones for early Solar System chronology and
785 genealogy. Geochim. Cosmochim. Acta 245, 577–596.
786 Savina M. R., Levine J., Stephan T., Dauphas N., Davis A. M., Knight K. B., Pellin M. J. (2010) Chromium
787 isotopes in presolar SiC grains. Lunar Planet. Sci. Conf. 41. abstr. #2568.
788 Schiller M., Van Kooten E., Holst J. C., Olsen M. B. and Bizzarro M. (2014) Precise measurement of
789 chromium isotopes by MC-ICPMS. J. Anal. At. Spectrom. 29, 1406–1416.
790 Schneider J. M., Burkhardt C., Marrocchi Y., Brennecka G. A. and Kleine T. (2020) Early evolution of the
791 solar accretion disk inferred from Cr-Ti-O isotopes in individual chondrules. Earth Planet. Sci. Lett. 551,
792 116585.
793 Shields, W. R., Murphy, T. J., Catanzaro, E. J., & Garner, E. L. (1966). Absolute Isotopic Abundance Ratios
794 and the Atomic Weight of a Reference Sample of Chromium. J. Res. Natl. Bur. Stand. A Phys. Chem. 70A,
795 193–197.
796 Shukolyukov A. and Lugmair G. (2006) Manganese–chromium isotope systematics of carbonaceous
797 chondrites. Earth Planet. Sci. Lett. 250, 200–213.
798 Shukolyukov A. and Lugmair G. W. (2004) Manganese-chromium isotope systematics of enstatite
799 meteorites. Geochim. Cosmochim. Acta 68, 2875–2888.
800 Shukolyukov A. and Lugmair G. W. (2000) On the ^{53}Mn Heterogeneity in the Early Solar System. In From
801 Dust to Terrestrial Planets (eds. W. Benz, R. Kallenbach, and G. W. Lugmair). Space Sciences Series of ISSI.
802 Springer Netherlands, Dordrecht. pp. 225–236.
803 Steele R. C. J., Coath C. D., Regelous M., Russell S. and Elliott T. (2012) Neutron-poor nickel isotope
804 anomalies in meteorites. ApJ 758, 59.
805 Stracke A., Palme H., Gellissen M., Münker C., Kleine T., Birbaum K., Günther D., Bourdon B. and Zipfel
806 J. (2012) Refractory element fractionation in the Allende meteorite: Implications for solar nebula

condensation and the chondritic composition of planetary bodies. Geochim. Cosmochim. Acta 85, 114–141.

Torrano Z. A., Brennecka G. A., Mercer C. M., Romaniello S. J., Rai V. K., Hines R. R. and Wadhwa M. (2023) Titanium and chromium isotopic compositions of calcium-aluminum-rich inclusions: Implications for the sources of isotopic anomalies and the formation of distinct isotopic reservoirs in the early Solar System. Geochim. Cosmochim. Acta 348, 309–322.

Trinquier A., Birck J. and Allegre C. J. (2007) Widespread ^{54}Cr Heterogeneity in the Inner Solar System. ApJ 655, 1179–1185.

Trinquier Anne, Birck J.-L. and Allègre C. J. (2008) High-precision analysis of chromium isotopes in terrestrial and meteorite samples by thermal ionization mass spectrometry. J. Anal. At. Spectrom. 23, 1565.

Trinquier A., Birck J.-L., Allègre C. J., Göpel C. and Ulfbeck D. (2008) ^{53}Mn–^{53}Cr systematics of the early Solar System revisited. Geochim. Cosmochim. Acta 72, 5146–5163.

Trinquier A., Elliott T., Ulfbeck D., Coath C., Krot A. N. and Bizzarro M. (2009) Origin of Nucleosynthetic Isotope Heterogeneity in the Solar Protoplanetary Disk. Science 324, 374–376.

Van Kooten E., Cavalcante L., Wielandt D. and Bizzarro M. (2020) The role of Bells in the continuous accretion between the CM and CR chondrite reservoirs. Meteorit. Planet. Sci. 55, 575–590.

Van Kooten E. M. M. E., Wielandt D., Schiller M., Nagashima K., Thomen A., Larsen K. K., Olsen M. B., Nordlund Å., Krot A. N. and Bizzarro M. (2016) Isotopic evidence for primordial molecular cloud material in metal-rich carbonaceous chondrites. Proc. Natl. Acad. Sci. U.S.A. 113, 2011–2016.

Vermeesch P. (2018) IsoplotR: A free and open toolbox for geochronology. Geosci. Front. 9, 1479–1493.

Wadhwa M., Zinner E. K. and Crozaz G. (1997) Manganese-chromium systematics in sulfides of unequilibrated enstatite chondrites. Meteorit. Planet. Sci. 32, 281–292.

Wang K., Moynier F., Podosek F. and Foriel J. (2011) ^{58}Fe and ^{54}Cr in early solar system materials. ApJ 739, L58.

Wang M., Audi G., Wapstra A. H., Kondev F. G., MacCormick M., Xu X. and Pfeiffer B. (2012) The AME2012 atomic mass evaluation. Chinese Physics C 36.

Warren P. H. (2011) Stable-isotopic anomalies and the accretionary assemblage of the Earth and Mars: A subordinate role for carbonaceous chondrites. Earth Planet. Sci. Lett. 311, 93–100.

Weisberg M. K. and Kimura M. (2012) The unequilibrated enstatite chondrites. Geochem. 72, 101–115.

Williams C. D., Sanborn M. E., Defouilloy C., Yin Q.-Z., Kita N. T., Ebel D. S., Yamakawa A. and Yamashita K. (2020) Chondrules reveal large-scale outward transport of inner Solar System materials in the protoplanetary disk. Proc. Natl. Acad. Sci. U.S.A. 117, 23426–23435.

Wood B. J., Smythe D. J. and Harrison T. (2019) The condensation temperatures of the elements: A reappraisal. Am. Min. 104, 844–856.

Yamakawa A. and Yin Q.-Z. (2014) Chromium isotopic systematics of the Sutter's Mill carbonaceous chondrite: Implications for isotopic heterogeneities of the early solar system. Meteorit. Planet. Sci. 49, 2118–2127.

Yamashita K., Maruyama S., Yamakawa A. and Nakamura E. (2010) ^{53}Mn-^{53}Cr chronometry of CB chondrite: evidence for uniform distribution of ^{53}Mn in the early solar system. ApJ 723, 20–24.

Yin Q.-Z., Jacobsen B. and Moynier F. (2007) Toward consistent chronology in the early solar system: high resolution ^{53}Mn-^{53}Cr chronology for chondrules. ApJ 662, L43–L46.

Yokoyama T., Ohkuma Y., Nishikawa K., Sumiya K. and Gautam I. (2023) Evaluation of the Residual Mass Fractionation in high-precision Cr Isotopic Analysis with TIMS. Geostand. Geoanal. Res. 47, 415–435.

Yokoyama, T., Wadhwa, M., Iizuka, T., Rai, V., Gautam, I., et al. 2023. Water circulation in Ryugu asteroid affected the distribution of nucleosynthetic isotope anomalies in returned sample. Science Advances, 9, eadi7048.

Zhu K., Moynier F., Schiller M. and Bizzarro M. (2020a) Dating and Tracing the Origin of Enstatite Chondrite Chondrules with Cr Isotopes. ApJ 894, L26.

Zhu K., Moynier F., Schiller M., Wielandt D., Larsen K. K., van Kooten E. M. M. E., Barrat J.-A. and Bizzarro M. (2020b) Chromium Isotopic Constraints on the Origin of the Ureilite Parent Body. ApJ 888, 126.

Zhu K., Moynier F., Schiller M., Alexander C. M. O., Davidson J., Schrader D. L., van Kooten E. M. M. E. and Bizzarro M. (2021) Chromium isotopic insights into the origin of chondrite parent bodies and the early terrestrial volatile depletion. Geochim. Cosmochim. Acta 301, 158–186.

Zinner E., Nittler L. R., Hoppe P., Gallino R., Straniero O. and Alexander C. M. O. 'D. (2005) Oxygen, magnesium and chromium isotopic ratios of presolar spinel grains. Geochim. Cosmochim. Acta 69, 4149–4165.

Zinner E., 2014. Presolar grains. In: Davis A.M. (Ed.), Meteorites and Cosmochemical Processes, vol. 1, Treatise on Geochemistry, 2nd ed. (exec. eds. Holland H.D., Turekian K.K.), pp. 181–213.

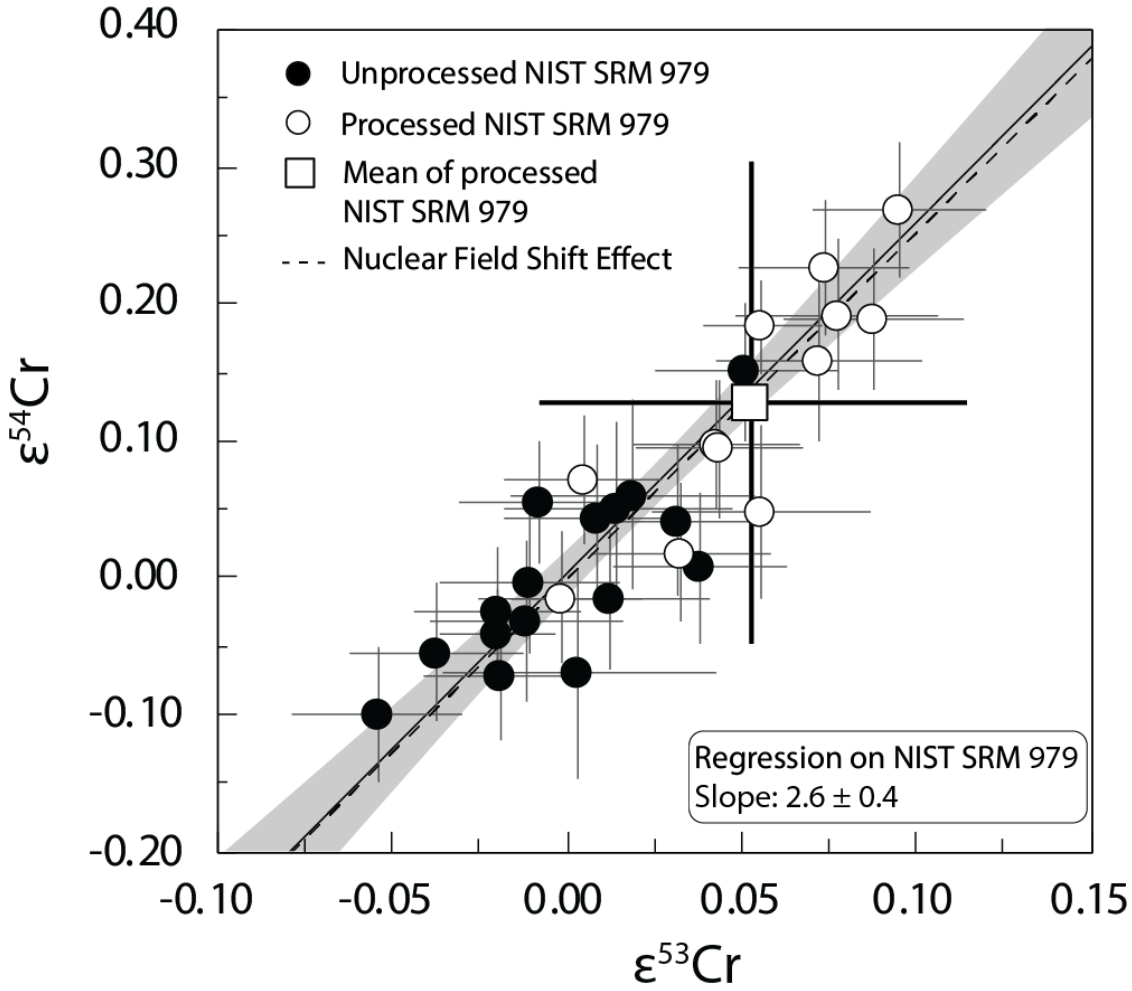

Figure 1: Chromium isotope composition of NIST SRM 979 standards unprocessed and processed with the same chemical procedure as the samples. The trend observed in the Cr isotope compositions coincides with the nuclear field shift effect calculated using Fujii et al. (2006) equations and nuclei masses from Wang et al. (2012) and mean-squared nuclear charge radii of Fricke and Heilig (2004). The regression line is obtained using IsoplotR (Vermeesch, 2018).

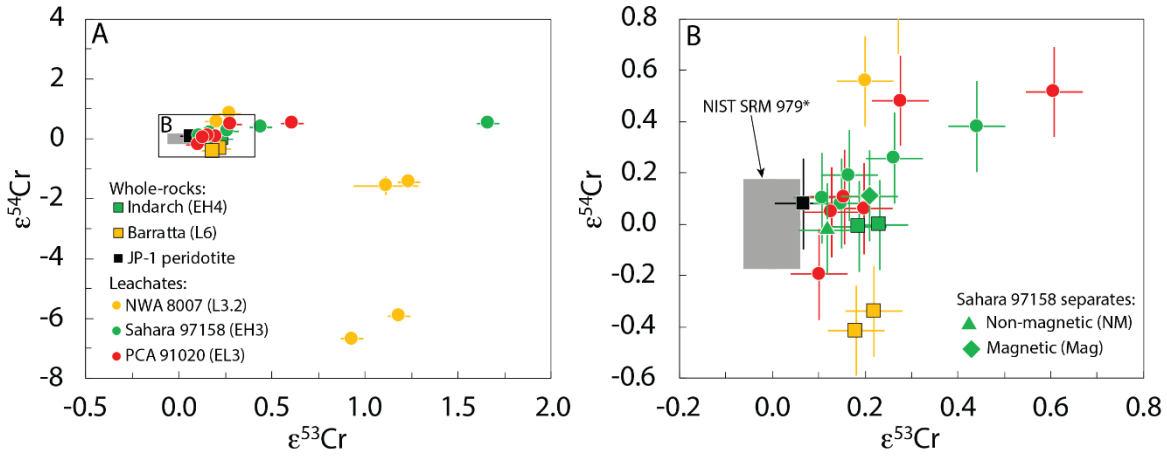

Figure 2: Chromium isotope composition of bulk chondrites and leachates of the ordinary chondrite NWA 8007 (L3.2) and the enstatite chondrites Sahara 97158 (EH3) and PCA 91020 (EL3). The grey area corresponds to twice the standard deviation on repeated measurements of processed NIST SRM 979 standards (NIST SRM 979*).

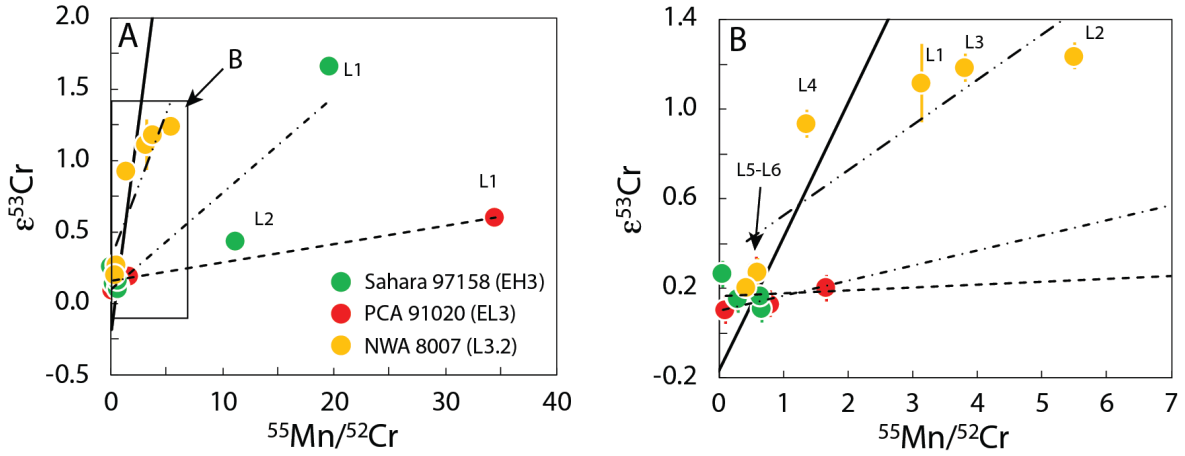

Figure 3: A) $\varepsilon^{53}Cr$ – $^{55}Mn/^{52}Cr$ isochron diagrams using leachates of each chondrite. Lines in the diagram are regressions obtained by Excel for the EH3 chondrite Sahara 97158 (dashed-dotted line), the EL3 chondrite PCA 91020 (dashed line) and the L3.2 chondrite NWA 8007 (dashed-double dotted line). The black line corresponds to the solar system isochron calculated using parameters from Göpel et al. (2015). Regression lines are not isochrons (see main text). B) Zoom-in corresponding to the delineated area in A) to show details.

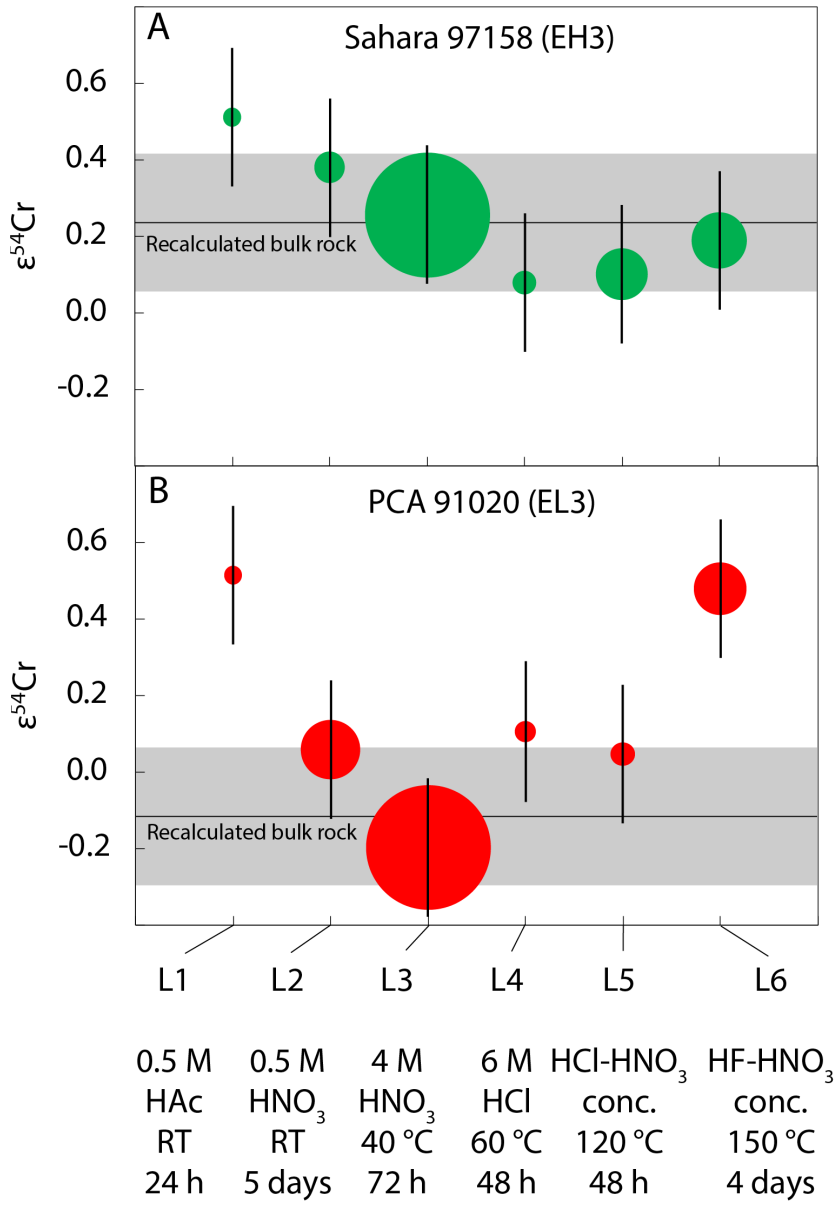

Figure 4: $\varepsilon^{54}Cr$ composition of each leachate step of the chondrites Sahara 97158 (EH3) in panel A, PCA 91020 (EL3) in panel B. The leaching procedure of the three chondrites is identical except for the last step (L6) for which PCA 91020 experienced a less aggressive dissolution (Table 1). The leaching steps mentioned on this figure are for Sahara 97158. The surface area of the data points is proportional to the Cr content distribution among leachates. The black line corresponds to the recalculated bulk rock using leachates and the error associated, represented with a grey area, corresponds to the external reproducibility of 18 ppm obtained from repeated measurements of processed NIST SRM 979 standard (NIST SRM 979*).

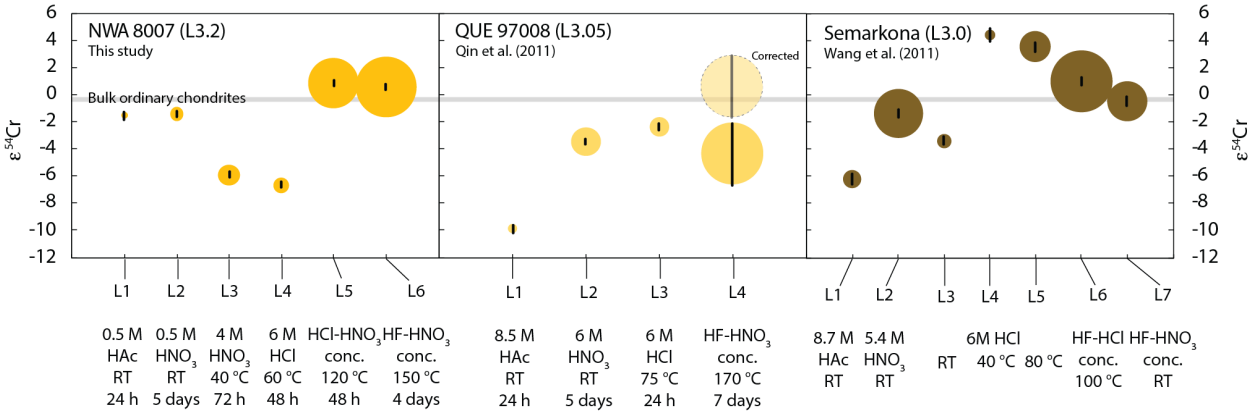

Figure 5: $\varepsilon^{54}Cr$ composition of leachates of ordinary chondrites from this study (NWA 8007 – L3.2), Qin et al. (2011a) (QUE 97008 – L3.05) and Wang et al. (2011) (Semarkona – L3.0). The surface area of the data points is proportional to the Cr content distribution among leachates. The shaded and dashed data point for L4 of QUE 97008 is the corrected value based on the bulk composition (see Qin et al., 2011 for details). The leaching procedures differ between the three studies and is reported on the horizontal axis. HAc: acetic acid; conc.: concentrated; RT: room temperature. The grey area corresponds to the bulk ordinary chondrite average of Zhu et al. (2021).

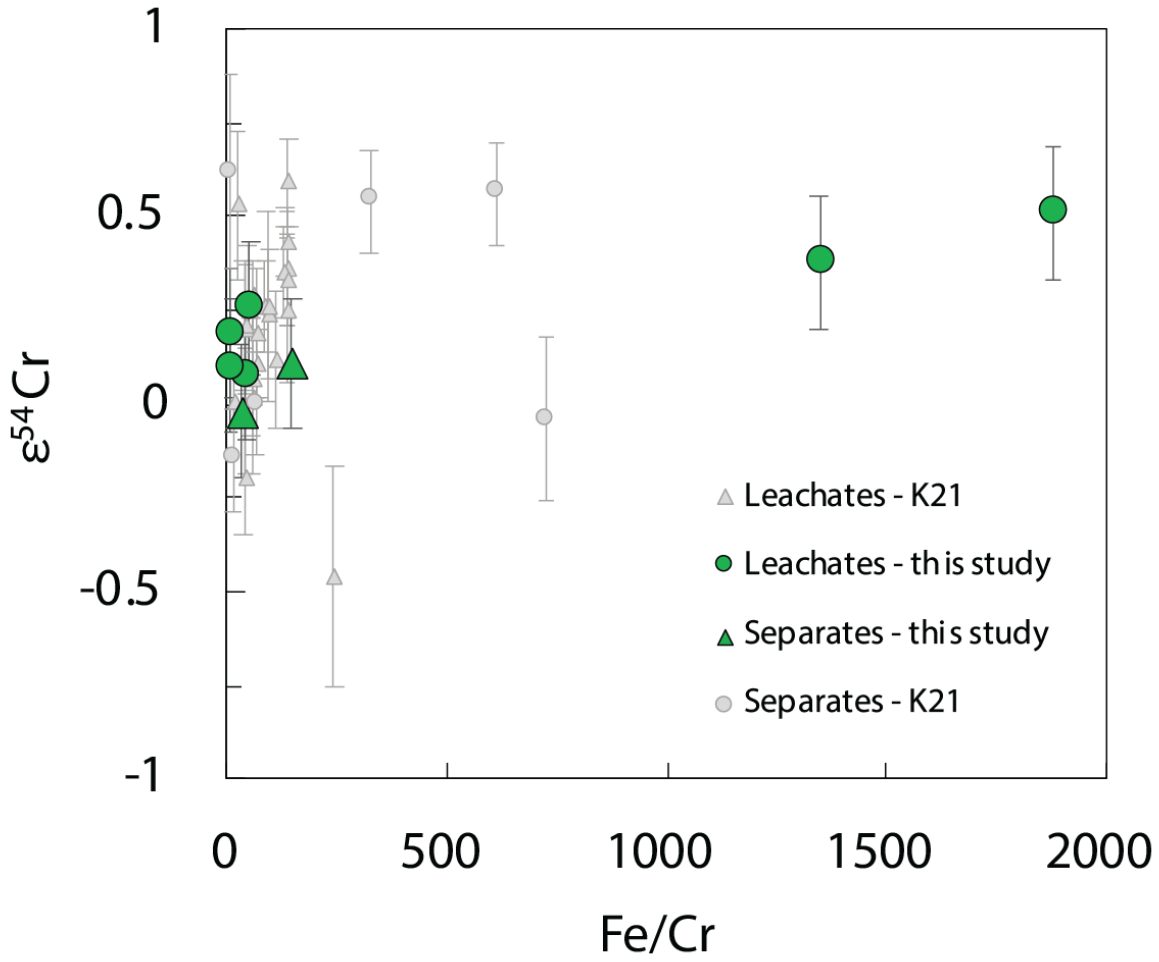

Figure 6: ε^{54}Cr composition and Fe/Cr ratios of the leachates and separates of EH3 chondrites from this study and Kadlag et al. (2021) (=K21). This study investigated Sahara 97158 and Kadlag et al. (2021) investigated Sahara 97072 and Kota-Kota. The leachates are more variable in their Fe/Cr and define shallower slopes in this diagram compared to separates. Co-variation of ε^{54}Cr and Fe/Cr ratios suggests that exposure to cosmic rays altered the ε^{54}Cr compositions.

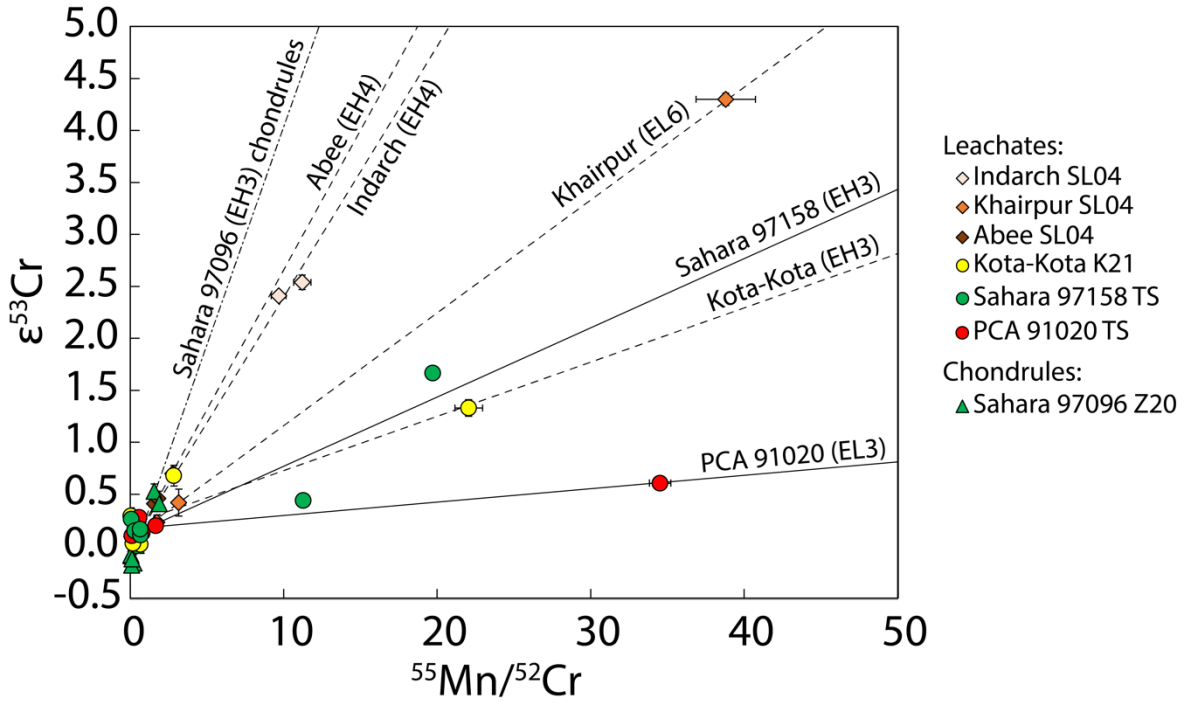

Figure 7: $\varepsilon^{54}Cr$-$^{55}Mn/^{52}Cr$ isochron diagrams with leachate and separates data of enstatite chondrites from this study and from the literature. Regression lines for each meteorite were obtained on leachates and chondrules using model 3 of IsoplotR. Also represented are separates obtained on EH3 chondrites which are not included in the regression lines. Leachates of Sahara 97158 (EH3) and PCA 91020 (EL3) are from this study (TS), leachates of Indarch (EH4), Khairpur (EL6) and Abee (EH4) were produced by Shukolyukov and Lugmair (2004) (SL04), leachates of Kota-Kota (EH3) by Kadlag et al. (2021) (K21) and chondrules from Sahara 97096 (EH3) by Zhu et al. (2020a) (Z20). The initial $^{53}Mn/^{55}Mn$ ratios determined using the isochrons of the chondrules of Sahara 97096, Abee, Indarch and Khairpur are $(5.01 \pm 0.59)\times10^{-6}$, $(3.0 \pm 0.4)\times10^{-6}$, $(2.8 \pm 0.1)\times10^{-6}$ and $(1.21 \pm 0.06)\times10^{-6}$, respectively. Regression lines using leachates of unequilibrated type 3 chondrites are erroneous and display low $^{53}Mn/^{55}Mn$ ratios compared to leachates of equilibrated chondrites and the chondrule isochron.

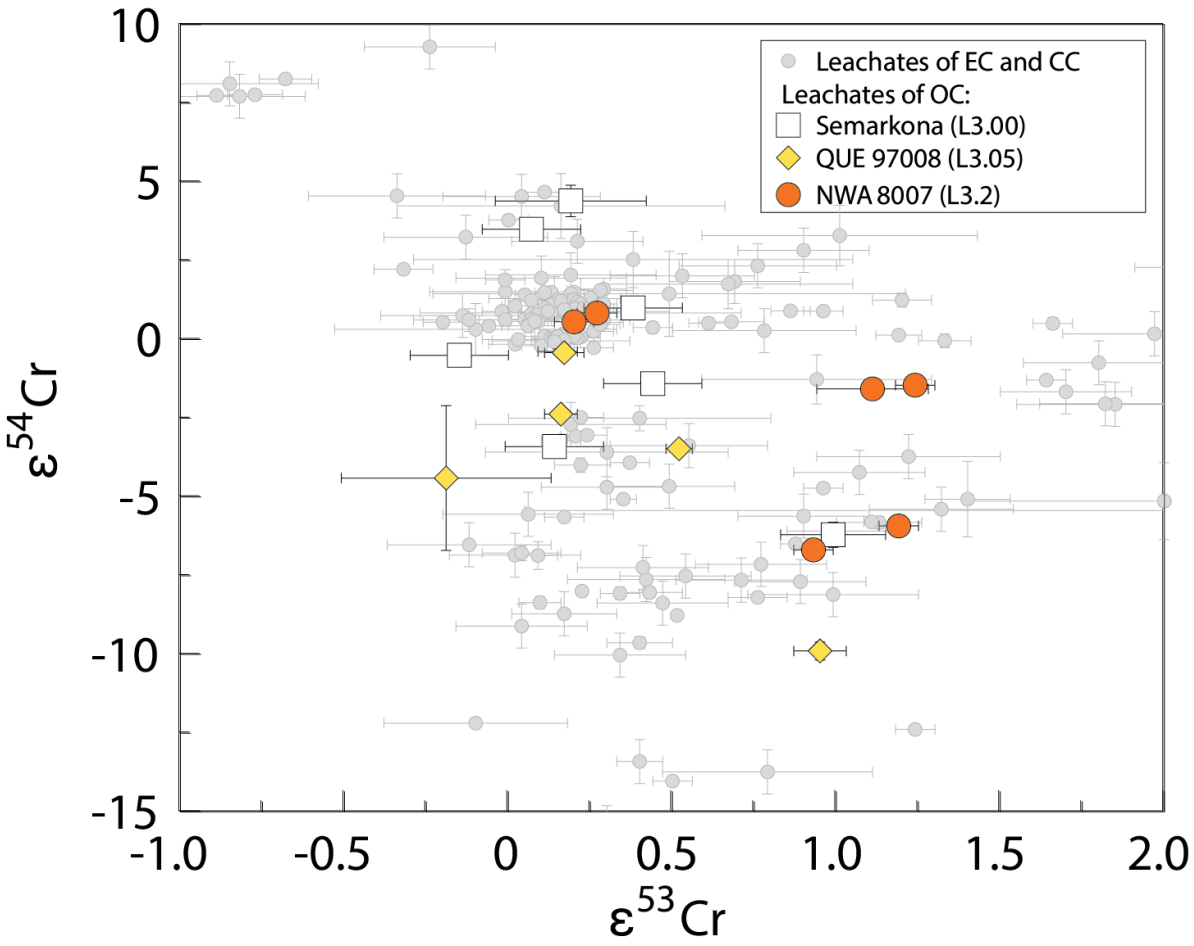

Figure 8: Chromium isotope composition of leachates of ordinary, enstatite, and carbonaceous chondrites from this study and the literature. The Cr isotope composition of the unequilibrated chondrites does not show a clear trend associated with their petrologic types (e.g. excesses in ε^{53}Cr). Leachate data are sourced from Rotaru et al. (1992), Trinquier et al. (2007), Petitat et al. (2011), Wang et al. (2011), Qin et al. (2011a), Yamakawa et al. (2014), Schiller et al. (2014), Göpel et al. (2015), Kadlag et al. (2021) and this study.

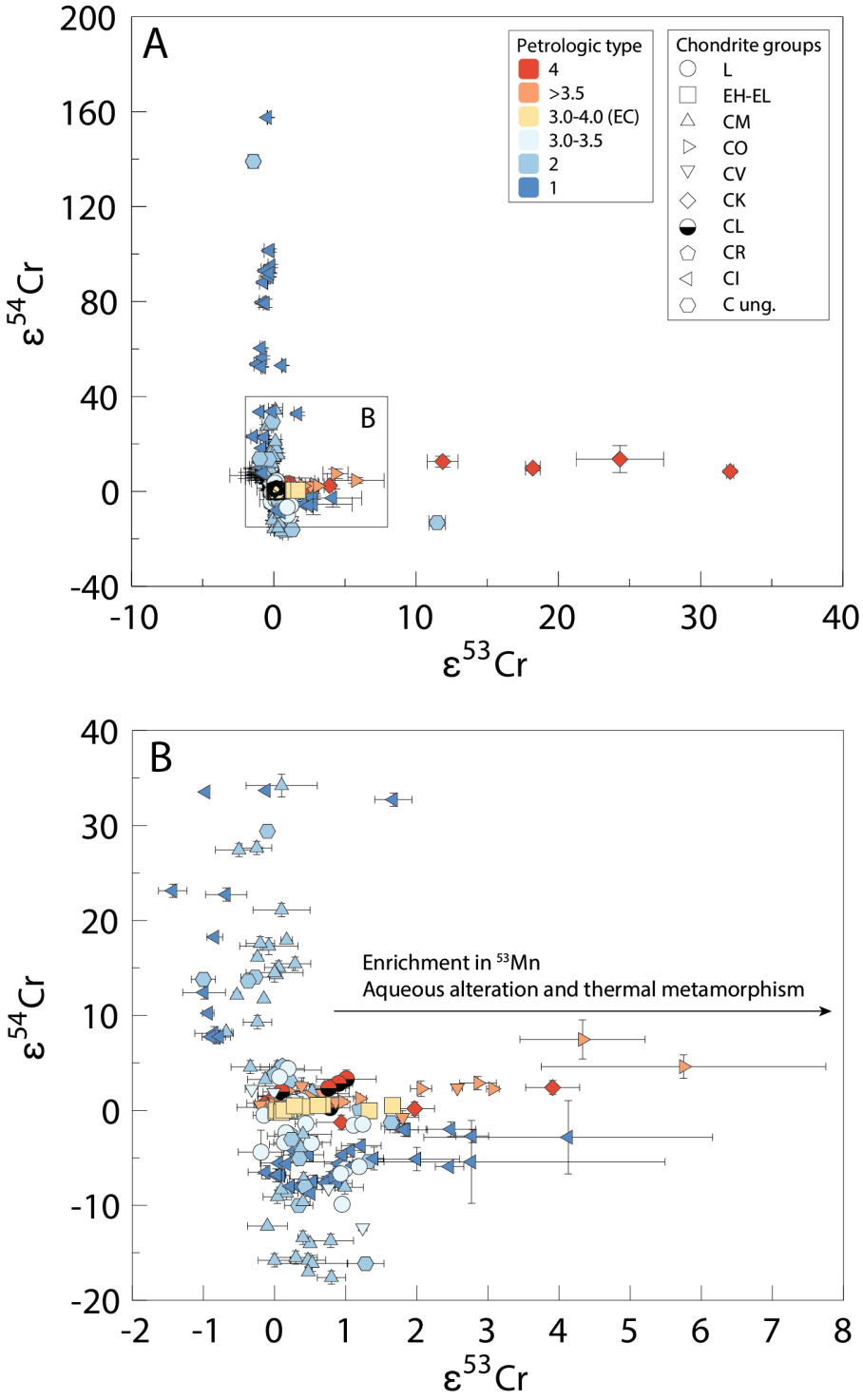

Figure 9: Chromium isotope composition of leachates of various chondrite types from this study and the literature. The data from Podosek et al. (1997) are not reported here due to larger errors, but nonetheless, these agree very well with other studies. The leachates are distinguished by meteorite group and petrologic type. The leachates of EC are classified as 3.0-4.0 as all samples have not been studied for their precise petrologic type. The EH3 chondrites typically range however from 3.1 to 3.7 in sub-types (Quirico et al., 2011). The data sources are the same as in Figure 8.

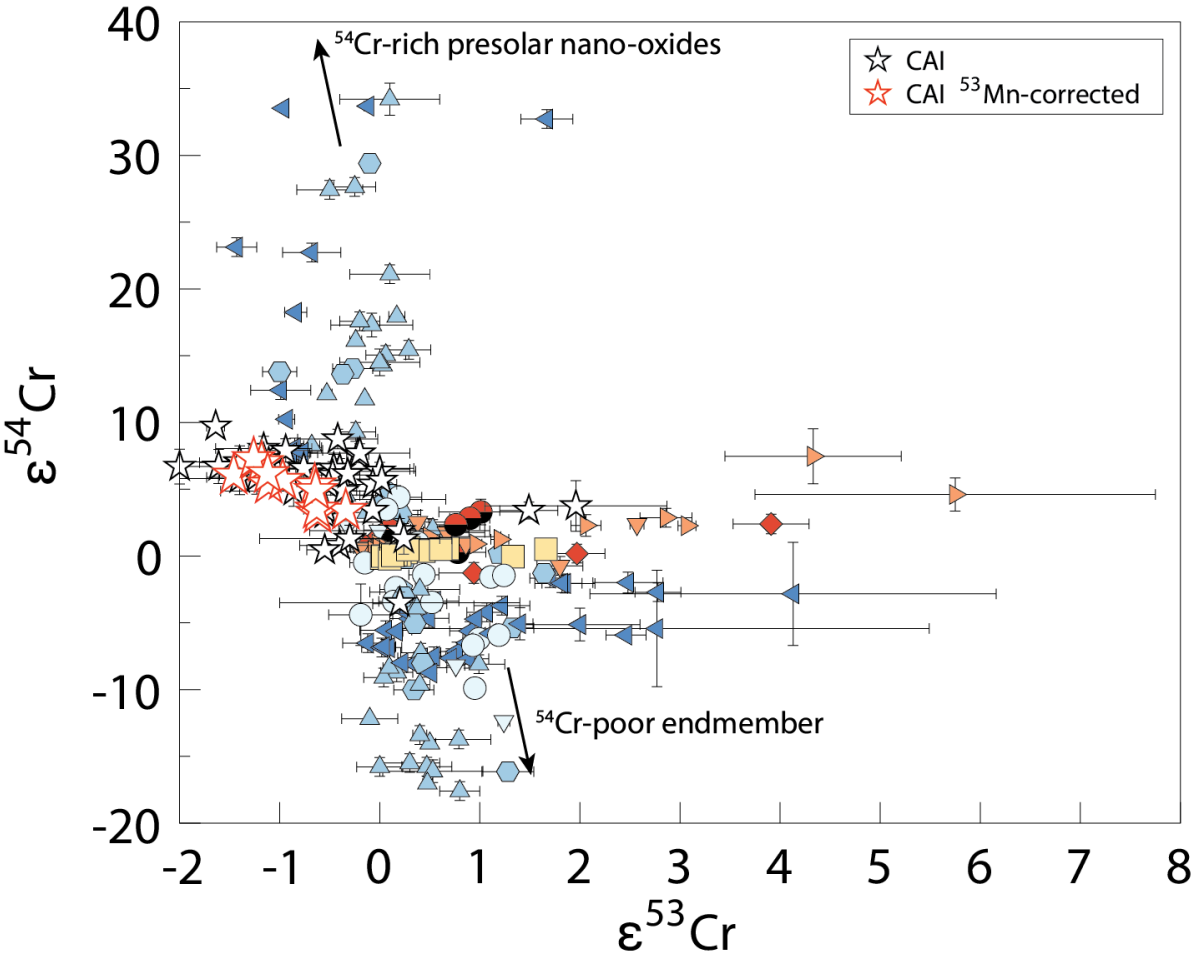

Figure 10: Chromium isotope composition of leachates of various types of chondrites and CAIs, from this study and the literature. Two main nucleosynthetic endmembers can explain the leachates' data. The CAIs plot off the trend with depletions in ε^{53}Cr and do not significantly contribute to the composition of the leachates of carbonaceous chondrites. Datapoints with red outlines are CAI with ε^{53}Cr corrected for ^{53}Mn decay from the study of Torrano et al. (2023). CAI data is sourced from Birck and Allègre (1985), Papanastassiou (1986), Birck and Lugmair (1988), Loss et al. (1994), Trinquier et al. (2008) and Torrano et al. (2023). The data sources for the leachates are the same as in Figure 8.

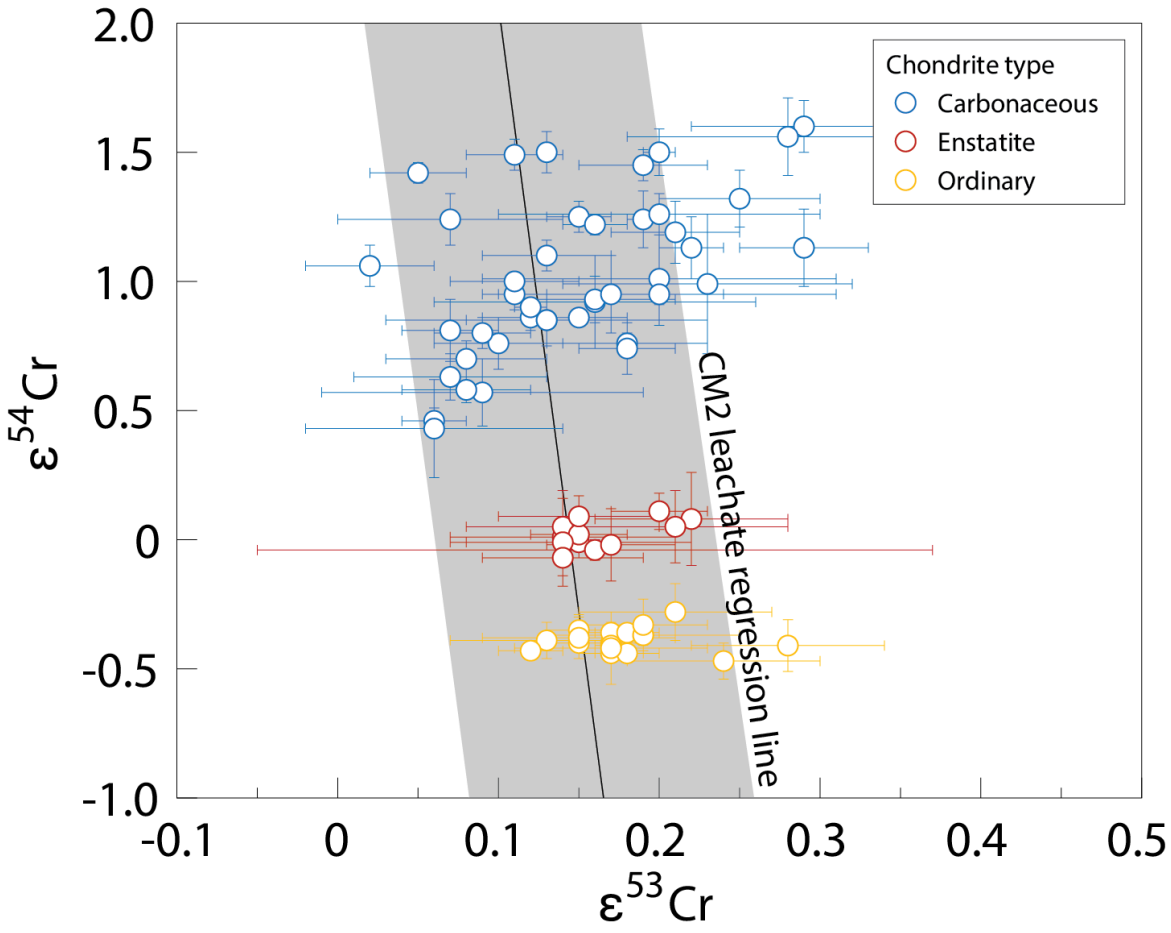

Figure 11: Chromium isotope composition of bulk chondrites. The regression line obtained on leachates of CM2 chondrites is shown and was calculated with the model 1 of IsoplotR. The slope is -47 ± 11 (MSWD = 17). Bulk chondrites data are sourced from the compilation of Zhu et al. (2021) and data are from Zhu et al. (2021), Schiller et al. (2014), Trinquier et al. (2007, 2008a), Yamashita et al. (2010), Qin et al. (2010), Göpel et al. (2015), Pedersen et al. (2019), Mougel et al. (2018), Petitat et al. (2011), Van Kooten et al. (2016, 2020), Sanborn et al. (2019), Zhu et al. (2020a, b), Langbroek et al. (2019), Jenniskens et al. (2012), Williams et al. (2020), Shukolyukov and Lugmair (2006), Moynier et al. (2007), Kadlag et al. (2019).

976 Table 1: Sequential dissolution procedure used in this study.

977

Step #	1	2	3	4	5	6[a]
Reagent	Acetic acid (HAc)	HNO_3	HNO_3	HCl	HCl-HNO_3	HF-HNO_3
Molarity	0.5 M	0.5 M	4 M	6 M	6 M – 15 M (2 :1)	28 M – 15 M (2 :1)
Temperature	Ambient	Ambient	40°C	60°C	120°C	150°C[b]/120°C[c]
Duration	24 h	24 h	72 h	48 h	48 h	96 h[b] / 48 h[c]
Digestion vessel	Savillex	Savillex	Savillex	Savillex	Savillex	Parr bomb[b] / Savillex[c]

978

979 [a] The procedure differs for step 6 between Sahara 97158, NWA 8007 and PCA 91020.

980 [b] Procedure for Sahara 97158 and NWA 8007.

981 [c] Procedure for PCA 91020.

982

983 Table 2: Chromium isotope composition of NIST SRM 979 Cr certified reference material and isotopic
984 standard.
985

	$I^{52}Cr$ (V)	$^{50}Cr/^{52}Cr$[a]	$^{53}Cr/^{52}Cr$	2SE	$^{54}Cr/^{52}Cr$	2SE	cycles
Processed NIST SRM 979 standards							
#1	10.6	0.05225	0.1134541	0.0000003	0.0282117	0.0000001	540
#2	11.0	0.05224	0.1134537	0.0000002	0.0282115	0.0000001	1080
#3	9.7	0.05222	0.1134539	0.0000003	0.0282114	0.0000002	440
#4	11.5	0.05230	0.1134534	0.0000003	0.0282110	0.0000001	540
#5	11.4	0.05227	0.1134535	0.0000003	0.0282112	0.0000001	540
#6	9.3	0.05230	0.1134537	0.0000004	0.0282111	0.0000002	360
#7	9.2	0.05226	0.1134539	0.0000003	0.0282115	0.0000002	460
#8	10.9	0.05229	0.1134539	0.0000003	0.0282116	0.0000001	540
#9	12.4	0.05231	0.1134531	0.0000003	0.0282111	0.0000001	540
#10	11.8	0.05229	0.1134530	0.0000003	0.0282109	0.0000001	540
#11	10.5	0.05227	0.1134535	0.0000003	0.0282112	0.0000001	540
#12	10.3	0.05224	0.1134540	0.0000003	0.0282115	0.0000001	540
Average			0.1134536		0.0282113		
2 SD			0.0000007		0.0000005		
2 RSD ppm			6.1		17.6		
2 SE			1.8		5.1		
Unprocessed NIST SRM 979 standards							
#1	9.7	0.05218	0.1134529	0.0000003	0.0282109	0.0000002	540
#2	10.8	0.05220	0.1134536	0.0000003	0.0282114	0.0000001	540
#3	11.2	0.05227	0.1134524	0.0000003	0.0282107	0.0000001	540
#4	9.8	0.05229	0.1134534	0.0000003	0.0282111	0.0000002	540
#5	12.5	0.05227	0.1134530	0.0000003	0.0282111	0.0000001	540
#6	10.3	0.05221	0.1134532	0.0000004	0.0282111	0.0000002	440
#7	10.6	0.05230	0.1134532	0.0000003	0.0282109	0.0000001	540
#8	9.7	0.05222	0.1134529	0.0000003	0.0282109	0.0000001	540
#9	9.6	0.05232	0.1134535	0.0000003	0.0282110	0.0000002	540
#10	10.6	0.05231	0.1134526	0.0000003	0.0282108	0.0000001	540
#11	9.9	0.05221	0.1134531	0.0000003	0.0282111	0.0000002	540
#12	8.6	0.05217	0.1134531	0.0000004	0.0282107	0.0000002	300
#13	9.8	0.05221	0.1134533	0.0000004	0.0282111	0.0000002	300
#14	12.0	0.05231	0.1134528	0.0000002	0.0282108	0.0000001	1080
#15	12.1	0.05236	0.1134528	0.0000003	0.0282107	0.0000001	540
#16	11.7	0.05232	0.1134528	0.0000003	0.0282109	0.0000001	540
Average		0.05226	0.1134530		0.0282109		
2 SD		0.00012	0.0000006		0.0000004		
2 RSD ppm			5.6		12.8		
2 SE			1.4		3.2		

986
987 [a] Average $^{50}Cr/^{52}Cr$ ratio, not corrected for mass fractionation.
988

989 Table 2: Chromium isotope composition of rock standard JP-1, bulk chondrites Indarch and Barratta, and
990 leachates and separates of the ordinary chondrite NWA 8007 and enstatite chondrites Sahara 97158 and
991 PCA 91020.
992

Sample	Cr (%)[a]	Fe/Cr	$^{55}Mn/^{52}Cr$	$I^{52}Cr$ (V)	$^{50}Cr/^{52}Cr$	$\varepsilon^{53}Cr$[b]	±[c]	$\varepsilon^{54}Cr$[b]	±[c]	n
Indarch #1				11.0	0.05230	0.19	0.06	-0.01	0.18	540
Indarch #2				9.7	0.05228	0.23	0.06	0.00	0.18	540
Barratta #1				11.8	0.05230	0.22	0.06	-0.34	0.18	540
Barratta #2				8.8	0.05224	0.18	0.06	-0.42	0.18	440
JP-1				13.0	0.05224	0.07	0.06	0.08	0.18	540
Sahara 97158 NM		33	0.65	9.6	0.05231	0.12	0.06	-0.02	0.18	420
Sahara 97158 Mag		149	0.72	10.1	0.05225	0.21	0.06	0.11	0.18	540
NWA 8007 L1	1 %	90	3.14	4.3	0.05169	1.11	0.17	-1.57	0.31	30
NWA 8007 L2	3 %	152	5.50	12.7	0.05223	1.24	0.06	-1.45	0.18	540
NWA 8007 L3	6 %	304	3.81	12.3	0.05220	1.19	0.06	-5.92	0.18	540
NWA 8007 L4	4 %	331	1.37	11.3	0.05223	0.93	0.06	-6.68	0.18	540
NWA 8007 L5	35 %	637	0.60	11.6	0.05214	0.27	0.06	0.84	0.18	240
NWA 8007 L6	52 %	9	0.44	11.3	0.05220	0.20	0.06	0.56	0.18	480
Sahara 97158 L1	1 %	1860	19.71	7.9	0.05231	1.66	0.06	0.51	0.18	200
Sahara 97158 L2	4 %	1335	11.27	12.3	0.05237	0.44	0.06	0.38	0.18	540
Sahara 97158 L3	69 %	53	0.07	9.3	0.05227	0.26	0.06	0.26	0.18	500
Sahara 97158 L4	2 %	44	0.30	9.8	0.05233	0.15	0.06	0.08	0.18	540
Sahara 97158 L5	11 %	5	0.67	11.6	0.05230	0.11	0.06	0.10	0.18	540
Sahara 97158 L6	13 %	6	0.65	10.8	0.05227	0.17	0.06	0.19	0.18	540
PCA 91020 L1	1 %		34.52	8.6	0.05206	0.61	0.06	0.52	0.18	160
PCA 91020 L2	14 %		1.67	11.7	0.05214	0.20	0.06	0.06	0.18	540
PCA 91020 L3	67 %		0.12	10.7	0.05236	0.10	0.06	-0.20	0.18	540
PCA 91020 L4	1 %		0.29	4.9	0.05219	0.16	0.08	0.11	0.18	80
PCA 91020 L5	2 %		0.80	9.8	0.05227	0.13	0.06	0.05	0.18	540
PCA 91020 L6	11 %		0.59	10.2	0.05213	0.28	0.06	0.48	0.18	540

993

994 [a] Proportion of Cr in each leachate relative to the total Cr content for each meteorite leached.

995 [b] Isotope compositions are reported relative to chemically processed NIST SRM 979 (NIST SRM 979*),
996 see methods.

997 [c] Errors are either the reproducibility determined on repeated analysis of NIST SRM 979* or twice the
998 standard error on the analysis, whichever is larger.

999